

Impacts of fire emissions and transport pathways

L. Huang et al.

Impacts of fire emissions and transport pathways on the interannual variation of CO in the tropical upper troposphere

L. Huang^{1,2}, R. Fu¹, and J. H. Jiang²

¹Jackson School of Geosciences, The University of Texas at Austin, Austin, TX, USA

²Jet Propulsion Laboratory, California Institute of Technology, Pasadena, CA, USA

Received: 30 August 2013 – Accepted: 11 September 2013 – Published: 7 October 2013

Correspondence to: L. Huang (leih@utexas.edu)

Published by Copernicus Publications on behalf of the European Geosciences Union.

Title Page

Abstract

Introduction

Conclusions

References

Tables

Figures

◀

▶

◀

▶

Back

Close

Full Screen / Esc

Printer-friendly Version

Interactive Discussion



Abstract

Carbon monoxide (CO) is an important tracer to study the transport of fire-generated pollutants from the surface to the upper troposphere (UT). This study analyzed the relative importance of fire emission, convection and climate conditions on the interannual variation of CO in the tropical UT, by using satellite observations, reanalysis data and transport pathway auto-identification method developed in our previous study. Empirical orthogonal function (EOF) and singular value decomposition (SVD) methods are used to identify the dominant modes of CO interannual variation in the tropical UT and factors that are related to these modes. Results show that the leading EOF mode is dominated by CO anomalies over Indonesia related to El Niño-Southern Oscillation (ENSO). This is consistent with previous findings by directly evaluating CO anomaly field. Transport pathway analysis suggests that the differences of UT CO between different ENSO types over the tropical continents are mainly dominated by the “local convection” pathway, especially the average CO transported by this pathway. The relative frequency of the “advection within the lower troposphere (LT) followed by convective vertical transport” pathway appears to be responsible only for the UT CO differences over the west-central Pacific between El Niño and La Niña years.

1 Introduction

Carbon monoxide (CO), which is a byproduct of the incomplete combustion of carbon-based fuels, plays an important role in atmospheric chemistry and radiation balance. CO is one of the ozone (O₃) precursors (Daniel and Solomon, 1998) and is also the primary sink of the hydroxyl radical (OH) (Thompson, 1992). With a lifetime of 1–2 months in the troposphere, CO is an excellent tracer to study the mass transport of polluted air originating in regions of biomass burning or fossil fuel combustion (Edwards et al., 2006a). Thus, understanding the factors that control CO temporal and spatial variations

ACPD

13, 25567–25615, 2013

Impacts of fire emissions and transport pathways

L. Huang et al.

Title Page

Abstract

Introduction

Conclusions

References

Tables

Figures

◀

▶

◀

▶

Back

Close

Full Screen / Esc

Printer-friendly Version

Interactive Discussion



is important to improve numerical model simulations and predictions of tropospheric ozone change and fire-generated pollutant transport.

Besides strong seasonal variations as shown by previous studies (Novelli et al., 1998; Schoeberl et al., 2006; Liu et al., 2007, 2010; Huang et al., 2012), CO has also been shown to have large interannual variability in the troposphere (Wotawa et al., 2001; Edwards et al., 2006b; Duncan and Logan, 2008; Liu et al., 2013). Edwards et al. (2006b) found that the interannual variation (IAV) of tropospheric CO in the Southern Hemisphere (SH) has a significant correlation with the El Niño–Southern Oscillation (ENSO) precipitation index. Duncan and Logan (2008) analyzed the factors that regulate the trends and interannual variability of tropospheric CO for 1988–1997 through a model study, and found the IAV of biomass burning, especially those major burning events in Indonesia associated with El Niño, is the main driver of large-scale CO variability in the tropics. Strong IAV of CO in the upper troposphere (UT) is found to be mainly related to the intense drought-induced fires in Indonesia and South America (Liu et al., 2013; Livesey et al., 2013).

Recent studies (e.g., Ashok et al., 2007; Kao and Yu, 2009; Kug et al., 2009) have shown that the canonical El Niño (eastern Pacific warming) has become less frequent and a different kind of El Niño (central Pacific warming) has become more common during the late twentieth century. These two types of El Niño have distinctively different anomalous large-scale circulation and convection patterns (Yeh et al., 2009; Su and Jiang, 2013), which would in turn have different impacts on CO transport to the UT. What are the differences between the impacts of different ENSO types on the IAV of tropical UT CO? The answer to this question may help to reconcile the discrepancies in previous studies about how ENSO would affect CO in the UT. For example, Chandra et al. (2009) attributed the change of UT CO to increased fires and meteorological changes over the Indonesian region during the 2006 El Niño, while Duncan et al. (2007) suggested that an increase of convective transport of CO emitted over South America and Africa due to an eastward shift of convective center in the Pacific closer to these

Impacts of fire emissions and transport pathways

L. Huang et al.

Title Page	
Abstract	Introduction
Conclusions	References
Tables	Figures
◀	▶
◀	▶
Back	Close
Full Screen / Esc	
Printer-friendly Version	
Interactive Discussion	



fires source regions also played an important role in the increase of UT CO during the 1997 El Niño.

Although fires in the tropical Africa and South America have important influence on the seasonal peaks of UT CO, how they would affect the IAV of UT CO has not been thoroughly investigated. Gonzi and Palmer (2010) suggested that the fractions of surface CO emissions transported to the UT are lower over Africa and South America than that over the tropical Asia. However, Ricaud et al. (2007) found that deep convection plays an important role in transporting CO to the UT over Africa, which suggests a change of emission and convection over this region could significantly influence UT CO. Thus, how changes of fire emissions over these two tropical continents contribute to the interannual changes of CO in the UT needs to be clarified.

Interannual variations of atmospheric circulation can also influence CO transport pathways (e.g., Duncan et al., 2007; Liu et al., 2013). The relative importance between changes of surface emission and transport pathways on the interannual changes of UT CO and how such relative importance varies with, for example, different ENSO types, is still an open question. Previous studies have shown that CO is transported from the surface to the UT through two pathways, i.e., the “local convection” pathway (Thompson et al., 1996; Pickering et al., 1996; Andreae et al., 2004), and the “lower troposphere (LT) advection → convection” pathway (Folkins et al., 1997; Andreae et al., 2001). The former refers to as that CO is transported from the surface to the UT by local deep convection over fire regions, whereas the latter refers to as that CO is advected from a fire region to a convective region within the LT, and then be uplifted to the UT by deep convection. This “LT advection → convection” pathway may be responsible for the fact that UT CO centers are often located above convective regions rather than fire regions. Huang et al. (2012) developed a method to automate the identification of these pathways through a joint use of A-Train multi-satellite measurements. This approach allows us to more efficiently evaluate the relationships between changes of CO emission, transport pathways and CO in the UT.

Impacts of fire emissions and transport pathways

L. Huang et al.

Title Page

Abstract

Introduction

Conclusions

References

Tables

Figures

◀

▶

◀

▶

Back

Close

Full Screen / Esc

Printer-friendly Version

Interactive Discussion



Impacts of fire emissions and transport pathways

L. Huang et al.

Title Page

Abstract

Introduction

Conclusions

References

Tables

Figures



Back

Close

Full Screen / Esc

Printer-friendly Version

Interactive Discussion



This study aims to investigate the dominant modes of the CO interannual variation in the tropical UT and their links to modes of interannual climate variability, such as ENSO and tropical Atlantic variability in determining the interannual variations of UT CO. In addition, the impacts of different ENSO types on CO transport to the UT are also evaluated. Section 2 of this paper introduces the data and methods used in this study. Section 3 identifies the dominant modes of the interannual variation of UT CO and evaluates the relative importance of CO emission, convection and continental regions that affect UT CO interannual variation over the tropics. The impacts of sea surface temperature (SST), convection and CO emission on UT CO interannual variation are analyzed in Sect. 4. The circulation pattern changes and the transport pathway differences associated with different ENSO types are investigated and discussed in Sect. 5. The main conclusions of this work are summarized and discussed in Sect. 6.

2 Data and methodology

2.1 Data

We use CO volume mixing ratio measurements from Aura Microwave Limb Sounder (MLS) to determine the concentration of CO in the UT, use MLS cloud ice water content (IWC) and CloudSat cloud water content (CWC) data to determine the strength of deep convection, and use CO emission data from the Global Fire Emission Database (GFED) to determine biomass burning emitted CO at the surface.

The MLS instrument is a small radio telescope aboard the Aura satellite, which was launched on 15 July 2004, and has a sun-synchronous orbit at an altitude of 705 km, with an equator crossing time at 1.45 a.m. and 1.45 p.m. local solar time and a 16-day repeat cycle. MLS observes many atmospheric components in the upper troposphere and lower stratosphere (UTLS) by measuring thermal emissions from broad spectral bands with a limb viewing geometry (Waters et al., 2006). MLS measurement has a vertical resolution of ~ 4 km for IWC and ~ 5 km for CO in the UTLS, and a horizontal

Impacts of fire emissions and transport pathways

L. Huang et al.

Title Page

Abstract

Introduction

Conclusions

References

Tables

Figures

◀

▶

◀

▶

Back

Close

Full Screen / Esc

Printer-friendly Version

Interactive Discussion



5 resolution of ~ 7 km across-track and 300–400 km along-track. We use Level 2 CO and IWC data derived according to the MLS Version 3.3 (V3.3) retrieval algorithm and screen the data using procedures as recommended in Livesey et al. (2011). These include the use of MLS IWC as a filter to exclude cloud-contaminated profiles in CO
10 data screening. The lowest usable retrieval level for CO and IWC is 215 hPa, where the estimated single-measurement precisions are ~ 20 ppbv for CO and ~ 1 mg m^{-3} for IWC. The earlier version of MLS CO (V2.2) was biased high by a factor of ~ 2 at 215 hPa (Livesey et al., 2008), but this bias has been largely eliminated in V3.3 CO data (Livesey et al., 2011). Only thick clouds which are typically associated with deep
15 convective cores are observable by MLS (Wu et al., 2008), thus MLS IWC is used as a proxy of deep convection in this study.

CloudSat was launched on 28 April 2006, which carries the first space-borne 94 GHz cloud profiling radar (CPR) to measure vertical profiles of cloud and precipitation properties, with a vertical resolution of 500 m (Stephens et al., 2002). The CloudSat measurements are reported on an increment of 240 m, with totally 125 vertical layers. The footprint of a single profile is approximately 1.7 km along-track by 1.3 km across-track, with an along-track sampling every 1.1 km (CloudSat Project, 2008). The CloudSat CWC is calculated as the sum of cloud ice water content and liquid water content observed by CloudSat. CWC is used as one of the proxies to estimate the relative strength
20 of convective activity.

The emission of CO by fire activity at the surface is obtained from the Global Fire Emission Database version 3 (GFED3) (van der Werf et al., 2010), currently available from 1997 to 2011. This gridded data has $0.5^\circ \times 0.5^\circ$ spatial resolution and monthly temporal resolution, and includes both burned area and fire emissions. Emissions of fire-generated trace gases are derived by combining satellite information on burned
25 area (Giglio et al., 2006, 2010), biogeochemical model estimates of fuel burned, and emission factors for each species. Burned area was derived primarily from the Moderate Resolution Imaging Spectroradiometer (MODIS) on Terra and Aqua satellites

(Giglio et al., 2006). The approach we used to derive daily emission of CO from GFED3 monthly emission is described in Mu et al. (2011).

Besides satellite observation data above, we also use monthly mean precipitation and SST data. The precipitation data is from the Global Precipitation Climatology Project (GPCP) (Adler et al., 2003), which is available from 1979 to 2011 and has a horizontal resolution of $2.5^\circ \times 2.5^\circ$. The SST data is obtained from the Optimum Interpolation (OI) SST Version 2 (V2) analysis produced by the National Oceanic and Atmospheric Administration (NOAA) using both in situ and satellite data (Reynolds et al., 2002), available from 1981 to present. The spatial resolution of SST data is $1^\circ \times 1^\circ$. In this paper, monthly anomaly of each variable is defined as the deviations from the corresponding climatological monthly mean. The climate indices used in this paper are obtained from <http://www.esrl.noaa.gov/psd/data/climateindices/list/> and http://www.jamstec.go.jp/frcgc/research/d1/iod/DATA/dmi_HadISST.txt.

To homogenize the horizontal resolutions of the MLS CO, IWC, SST and GFED CO emission, we averaged these data into 4° latitude \times 8° longitude grid boxes. The MLS CO and IWC data were also averaged over each month to get the monthly mean.

2.2 Methodology

The Empirical Orthogonal Function (EOF) analysis has been widely used to extract individual modes of variability from data with complex spatial/temporal structures, since the first introduction by Lorenz (1956). Rotated EOF (REOF) is a technique simply based on rotating EOFs. It has been adopted by atmospheric scientists since the mid-80th (Richman, 1986) as an attempt to overcome some of the EOF shortcomings (e.g., domain dependence, difficulty of physical interpretability). To identify the dominant modes of the interannual variation of CO in the tropical UT (30° S– 30° N), we apply the REOF analysis to the monthly anomalies of MLS CO at 147 hPa, for the period of August 2004 to July 2012. After that, we apply the Singular Value Decomposition (SVD, Wallace et al., 1992) analysis between CO anomalies at 147 hPa and SST anomalies in the tropics, to determine the leading SVD modes that dominate the

Impacts of fire emissions and transport pathways

L. Huang et al.

Title Page

Abstract

Introduction

Conclusions

References

Tables

Figures



Back

Close

Full Screen / Esc

Printer-friendly Version

Interactive Discussion



Impacts of fire emissions and transport pathways

L. Huang et al.

[Title Page](#)[Abstract](#)[Introduction](#)[Conclusions](#)[References](#)[Tables](#)[Figures](#)[◀](#)[▶](#)[◀](#)[▶](#)[Back](#)[Close](#)[Full Screen / Esc](#)[Printer-friendly Version](#)[Interactive Discussion](#)

squared covariance of the two fields. SVD identifies the leading modes based on their fractions of the total squared covariance between two fields, typically referred to as the left and right field. The spatial pattern of a SVD mode projected on the left and right field, respectively, can be obtained from the homogeneous correlation map between one field and its own principle component of that SVD mode. The correlation between these two fields for a SVD mode can be obtained from the heterogeneous correlation maps, for the left and right field, respectively. The heterogeneous correlation map for the left (right) field represents the correlation between the left (right) field and the principle component of the right (left) field. We also apply the SVD analysis to determine the field correlations between anomalies of UT CO and anomalies of convection and CO emission, respectively. In this way, we can evaluate how IAVs of SST, convection and CO emission influence the IAV of CO in the tropical UT.

The relative importance of different climate conditions on the significant REOF and SVD modes of CO in the tropical UT is determined using correlation analysis. Since ENSO and some of the other climate indices are known to have strong autocorrelation, it is important to estimate the influence of autocorrelation on the significance of the correlation coefficients. To address the autocorrelation issue, we use both Livezey and Chen (1983) and Bretherton et al. (1999)'s methods to calculate the effective degrees of freedom (DOFs) for a time series, and the results are the same for both methods. The circulation pattern changes associated with different ENSO types are analyzed using composite analysis. The pathway auto-identification method developed in Huang et al. (2012) is used in this study to characterize the differences of CO transport between El Niño and La Niña years. This method streamlines the identification of two CO transport pathways by combining instantaneous along-track observations of CO in the UT from the Aura MLS, convective clouds from the CloudSat radar, and CO emissions derived from the MODIS fire counts data. Further details about this method can be found in Huang et al. (2012).

3 Regions affecting UT CO interannual variation

Figures 1–3 shows the results of REOF analysis for the monthly anomalies of tropical UT CO at 147 hPa from August 2004 to July 2012. The first 10 EOF eigenvalues along with their uncertainties based on a “rule of thumb” (North et al., 1982) are shown in Fig. 1a. Only the first three eigenvalues are well separated from the rest, together they account for 64.5% of the total monthly UT CO variance. Individually, they explain 37.6%, 18.6% and 8.3% of the total variance. The rotated EOF analysis was performed using an orthogonal method (varimax), keeping the first 10 EOFs. The spatial patterns associated with the first three rotated EOF modes are shown as homogeneous correlation maps E1, E2 and E3 (Figs. 1–3c), while the temporal variations of each eigenvector are represented by the rotated principal components PC1, PC2 and PC3 (Figs. 1–3b). The correlation coefficients between each PC and climate indices are listed in Table 1. E1 shows two high-correlation centers located over the tropical Indian Ocean, Indonesia and South Pacific. Since the square of the correlation represents the variance explained locally, this mode accounts for up to 96% of the variance in the regions of largest amplitude. PC1 is significantly correlated (at 90% confidence level, hereinafter) with the ENSO indices (e.g., Niño4, SOI, as shown in Table 1), after considering the effective DOFs associated with autocorrelation (hereinafter). This suggests that the first REOF mode of UT CO interannual variation is mainly dominated by ENSO. E2 shows a high-correlation center located over South America (Fig. 2c), which explains up to 86% of the variance over this region. PC2 is significantly correlated with the Atlantic Ocean indices (e.g., AMO, NAO). Thus, the second EOF mode probably represents the significant influence of the Atlantic Ocean. E3 shows a high-correlation center over West Africa and tropical Atlantic Ocean, with explanation of up to 86% of the variance (Fig. 3c). PC3 is significantly correlated with multiple climate indices (Table 1), suggesting this mode is affected by various climate conditions. Overall, this REOF analysis suggests that the interannual variation of tropical UT CO is significantly affected by changes over the three tropical land regions and various climate condi-

Impacts of fire emissions and transport pathways

L. Huang et al.

Title Page

Abstract

Introduction

Conclusions

References

Tables

Figures

◀

▶

◀

▶

Back

Close

Full Screen / Esc

Printer-friendly Version

Interactive Discussion



tions. The changes of UT CO over tropical Asia have the largest contribution, whereas those over South America and Africa have a secondary but still significant contribution. Among all the climate conditions, ENSO has the largest impact.

To further evaluate the relative importance of emission and convection on the UT CO interannual variation, we analyzed the time series of monthly anomalies of GFED CO emissions, MLS CO at 147 hPa and IWC at 215 hPa over South America (15° S–12° N, 85° W–32° W), Central Africa (15° S–15° N, 20° W–50° E), SE Asia (10° S–15° N, 90° E–160° E) and the Tropics (15° S–15° N, 180° W–180° E). Here 215 hPa IWC is used as a proxy of deep convection (Jiang et al., 2007, 2011). Over the Tropics (Fig. 5b), UT CO anomaly is significantly correlated with CO emission anomaly, and the largest correlation coefficient occurs at 2-month time lag ($r = 0.64$). The correlation with IWC anomaly is relatively weak at zero time lag ($r = 0.31$). However, during some period (e.g., October 2010–January 2011), there is overlap between peaks of UT CO anomaly and IWC anomaly. This suggests that while surface CO emission controls most of the UT CO anomalies, sometimes convective transport is also important. To evaluate the IAV of UT CO in different subregions, we also examined the three tropical continents. Over South America (Fig. 4a), UT CO anomaly is significantly correlated with CO emission anomaly, and the correlation coefficient is largest at 2-month time lag ($r = 0.72$). The IWC anomaly has a weak correlation ($r = 0.25$) with UT CO anomaly at zero time lag. This is similar to the Tropics, suggesting that the IAV of UT CO over this region mainly follows the changes of surface CO emission, which is consistent with previous studies (Liu et al., 2010). Over Central Africa (Fig. 4b), UT CO anomaly is only significantly correlated with IWC anomaly ($r = 0.39$), not with CO emission. Thus, the IAV of UT CO over this region is mainly influenced by changes of convective transport, instead of CO emission anomaly. Over SE Asia (Fig. 5a), both CO emission and IWC anomalies are significantly correlated with UT CO anomaly (0.77 and -0.66 , respectively), suggesting that both CO emission and convective transport are important in determining the IAV of UT CO over this region.

Impacts of fire emissions and transport pathways

L. Huang et al.

Title Page

Abstract

Introduction

Conclusions

References

Tables

Figures

◀

▶

◀

▶

Back

Close

Full Screen / Esc

Printer-friendly Version

Interactive Discussion



4 Impacts of SST, convection and CO emission on UT CO interannual variation

We use SVD method to study the field relationships between UT CO anomaly and the anomalies of SST, convection and CO emission during the period August 2004–December 2011. In contrast to the individual EOF analysis performed on the UT CO (Sect. 3), the SVD analysis on two combined fields will identify only these modes of behavior in which the two fields are strongly coupled.

The first three SVD modes between 147 hPa CO anomaly and SST anomaly account for 64.9%, 16.3% and 10.1% of the total squared covariance, respectively. The covariance explained by the rest modes is much smaller compared to the first three modes; thus we only discuss these three modes here. Figure 6a shows the two PC time series of the first SVD mode of 147 hPa CO and SST. The correlation coefficient between the two PCs is 0.65, which is an indicator of the coupling strength. The correlation coefficients between each PC and climate indices are listed in Table 2. Both PCs have significant correlation with ENSO indices (Niño 3, Niño 4, Niño 3.4 and SOI) and Pacific Decadal Oscillation (PDO) index. However, the largest correlation is with Niño 4, 0.53 for UT CO and 0.87 for SST. This suggests the SST anomaly of central tropical Pacific (Niño 4) may have larger influence on UT CO interannual variation than that of eastern tropical Pacific (Niño 3). The coupled spatial patterns of the first SVD mode are shown in Fig. 6b and c as homogeneous correlation maps for UT CO and SST respectively, and in Fig. 6d as heterogeneous correlation map for UT CO. The homogeneous correlation map of UT CO resembles that of the first REOF mode of UT CO (Fig. 1c), while the homogeneous correlation map of SST shows two dipoles: one is a west-central Pacific dipole, and the other is a northwest–southeast Indian Ocean dipole. This map also shows a tri-pole over the Atlantic Ocean, with the SST anomaly over the equatorial Atlantic Ocean off-phase with those over the northern and southern subtropical Atlantic Ocean. The SST anomaly dipoles and tri-pole are consistent with the ENSO related SST changes (Enfield and Mestas-Nuñez, 2000). The heterogeneous correlation map of UT CO shows a zonal dipole between the tropical Asia and

Impacts of fire emissions and transport pathways

L. Huang et al.

Title Page

Abstract

Introduction

Conclusions

References

Tables

Figures



Back

Close

Full Screen / Esc

Printer-friendly Version

Interactive Discussion



South America-southern Africa, which again resembles that of the first REOF mode of UT CO and suggests the dependence of UT CO on SST is mainly affected by ENSO.

The results of the second SVD mode of 147 hPa CO and SST are shown in Fig. 7. The correlation coefficient between the two PCs is 0.64 (Fig. 7a). As shown in Table 2, there is no climate index that has significant correlation with both PCs. The homogeneous correlation map of UT CO (Fig. 7b) shows a center of high correlation over the Atlantic Ocean, while the homogeneous correlation map of SST (Fig. 7c) resembles that of the first SVD. The heterogeneous correlation map of UT CO (Fig. 7d) shows high correlation over the tropical Atlantic Ocean and West Africa, which resembles that of the third REOF mode of UT CO (Fig. 3c). Thus, the second SVD mode may indicate the influence of the Atlantic Ocean. For the third SVD mode of 147 hPa CO and SST (not shown), the correlation coefficient between the two PCs is 0.73. Both PCs have significant correlation with 5 climate indices (Table 2), and the largest correlation is with TNA (0.50 for UT CO and 0.76 for SST). The heterogeneous correlation map of UT CO shows high correlation over the Northeast Pacific and North Atlantic Ocean.

The first three SVD modes between 147 hPa CO anomaly and 215 hPa IWC anomaly account for 65.0 %, 14.3 % and 7.9 % of the total squared covariance, respectively. The correlation coefficient between the two PCs of the first SVD mode is 0.74 (Fig. 8a). Both PCs have significant correlation with ENSO indices (Niño 3, Niño 4, Niño 3.4 and SOI) and PDO (Table 3), and the strongest correlation is with Niño 4. Thus, it suggests the central tropical Pacific SST anomaly has the strongest influence on the IAV of UT CO, similar to the first SVD mode between UT CO and SST. The coupled spatial patterns of the first SVD mode are shown in Fig. 8b and c as homogeneous correlation maps for UT CO and IWC respectively, and in Fig. 8d as heterogeneous correlation map for UT CO. All three maps are quite similar to those of the first SVD mode between UT CO and SST, except a larger center of negative correlation over the tropical Atlantic Ocean in the homogeneous correlation map for IWC. The heterogeneous correlation map of UT CO again resembles that of the first REOF mode of UT CO (Fig. 1c) and suggests the dependence of UT CO on convection is mainly affected by ENSO.

Impacts of fire emissions and transport pathways

L. Huang et al.

Title Page

Abstract

Introduction

Conclusions

References

Tables

Figures

◀

▶

◀

▶

Back

Close

Full Screen / Esc

Printer-friendly Version

Interactive Discussion



Impacts of fire emissions and transport pathways

L. Huang et al.

Title Page

Abstract

Introduction

Conclusions

References

Tables

Figures



Back

Close

Full Screen / Esc

Printer-friendly Version

Interactive Discussion



For the second SVD mode of 147 hPa CO and 215 hPa IWC, the correlation coefficient between the two PCs is 0.60 (Fig. 9a). As shown in Table 3, there is no climate index that has significant correlation with both PCs. The homogeneous correlation map of UT CO (Fig. 9b) shows a center of high correlation over the South Atlantic Ocean, while the homogeneous correlation map of IWC (Fig. 9c) shows a center over the Amazon and tropical Atlantic Ocean. The heterogeneous correlation map of UT CO (Fig. 9d) shows high correlation over the Central Atlantic Ocean and West Africa, which is similar to that of the second SVD mode between 147 hPa CO and SST. For the third SVD mode of 147 hPa CO and 215 hPa IWC (not shown), the correlation coefficient between the two PCs is 0.70. Both PCs have significant correlation with 2 climate indices (Table 3), and the largest correlation is with TNA, 0.43 for UT CO and 0.37 for IWC. The heterogeneous correlation map of UT CO is similar to that of the third SVD mode between 147 hPa CO and SST.

The first three SVD modes between 147 hPa CO anomaly and CO emission anomaly account for 88.1 %, 4.8 % and 3.4 % of the total squared covariance, respectively. The correlation coefficient between the two PCs of the first SVD mode is 0.60 (Fig. 10a). Both PCs have significant correlation with ENSO index (SOI) (Table 4). The coupled spatial patterns of the first SVD mode are shown in Fig. 10b and c as homogeneous correlation maps for UT CO and CO emission respectively, and in Fig. 10d as heterogeneous correlation map for UT CO. All three maps show a center of high correlation over Indonesia and the adjacent Indian Ocean (except the CO emission map since there is no emission over ocean), suggesting the dominance of this region in tropical UT CO interannual variation.

For the second SVD mode of 147 hPa CO and CO emission, the correlation coefficient between the two PCs is 0.38 (Fig. 11a). As shown in Table 4, both PCs have significant correlation with only AMO, 0.45 for UT CO and 0.25 for CO emission. The homogeneous correlation map of UT CO (Fig. 11b) shows high correlation over South America and South Atlantic Ocean, while the homogeneous correlation map of CO emission (Fig. 11c) also shows a center over South America. However, the heteroge-

neous correlation map of UT CO (Fig. 11d) only shows relatively weak correlation over the southern Africa. For the third SVD mode of 147hPa CO and CO emission (not shown), the correlation coefficient between the two PCs is 0.39 and no climate index is significantly correlated with both PCs (Table 4).

The SVD analyses above suggested that ENSO is the dominant climate condition that affects the field relationship between UT CO and SST, convection, and CO emission. The similarity between SVD analyses of CO-SST and CO-IWC suggests that SST anomaly plays an important role in deep convection changes. AMO has significant impact on the field relationship between UT CO and CO emission as it shows up in the second SVD mode, possibly through its impact on the rainfall in South America and Africa (Knight et al., 2006). Since ENSO is the dominant factor governing the interannual variation of tropical UT CO, we need to investigate the impacts of different types of ENSO on CO transport to the UT.

5 Impact of ENSO types on UT CO interannual variation

Since the launch of Aura, there have been several ENSO periods: 2004, 2006 and 2009 are typical El Niño-like years, while 2005, 2007 and 2010 are typical La Niña years (based on a threshold of $\pm 0.5^{\circ}\text{C}$ for the Oceanic Niño Index (ONI), http://www.cpc.ncep.noaa.gov/products/analysis_monitoring/ensostuff/ensoyears.shtml). Figure 12 shows the SST anomalies during the mature phase (DJF) of each ENSO year. Besides the sign differences of SST anomaly in the central-eastern Pacific between El Niño and La Niña years, there are also large differences in the location and strength of the maximum SST anomaly. For the 2004/2005 and 2009/2010 El Niño, the strong positive SST anomalies were mainly located in the central Pacific, while in 2006/2007 El Niño, there were also strong SST anomalies in the eastern Pacific. Thus, these three periods represent two different types of El Niño, which have been referred by previous studies as CP-El Niño and EP-El Niño (e.g., Yeh et al., 2009; Lee et al., 2010; Su and Jiang, 2013). The 2009/2010 El Niño was much stronger than

Impacts of fire emissions and transport pathways

L. Huang et al.

Title Page

Abstract

Introduction

Conclusions

References

Tables

Figures

◀

▶

◀

▶

Back

Close

Full Screen / Esc

Printer-friendly Version

Interactive Discussion



the former two El Niños, as shown by the larger and more extensive SST anomalies. For the three La Niña periods, the intensity became stronger one after another, as indicated by the negative SST anomalies extending from the equator to the subtropics.

Since the strongest biomass burning in South America and Central Africa occurs in boreal fall (Huang et al., 2012), here we choose September–November (SON) as the focused period to study the differences of CO transport to the UT between different ENSO types. The distributions of seasonal average CO and IWC anomalies at 215 hPa are shown in Fig. 13. The anomalies are calculated as the seasonal mean of each year minus the 2005–2011 climatological mean. In general, UT CO shows positive anomalies over the Indonesian region and Indian Ocean in El Niño years, compared to negative anomalies over the same region in La Niña years. In addition, UT CO shows consistently strong positive anomalies over South America in La Niña years, while the anomalies are not consistent in El Niño years. For example, there were moderate positive UT CO anomalies in 2004, compared to strong negative anomalies in 2009 over South America. Over Indonesia, UT CO anomaly generally shows opposite sign to that of co-located IWC, consistent with the negative correlation between UT CO and IWC anomalies over SE Asia as discussed before. Over South America, the CO anomaly centers are not co-located with the centers of IWC anomaly. Another region that shows distinct ENSO impact is the central Pacific (around the dateline), where positive (negative) UT CO and IWC anomalies are co-located during El Niño (La Niña) years, suggesting that convective transport is important in determining UT CO concentration over this region.

Why are the patterns of the UT CO anomalies so different between different ENSO types? To explore this question, we carried out the analyses through two ways: one way is to analyze the differences of surface emission and convection, and the other way is to analyze the differences of CO transport pathways. The distributions of GFED CO emission and GPCP precipitation anomalies are shown in Fig. 14. During El Niño periods, CO emission shows positive anomalies over Indonesia and northern Australia, and negative anomalies over South America. The positive emission anomalies are from

Impacts of fire emissions and transport pathways

L. Huang et al.

Title Page

Abstract

Introduction

Conclusions

References

Tables

Figures

◀

▶

◀

▶

Back

Close

Full Screen / Esc

Printer-friendly Version

Interactive Discussion



intense fires caused by drought conditions related to ENSO (e.g., Logan et al., 2008; Chandra et al., 2009), which are consistent with the co-located negative precipitation anomalies. However, 2009 El Niño is an exception. There was a negative emission anomaly over Indonesia, and a much stronger negative anomaly over South America than previous two events. This may be the reason for the weak CO anomaly over Indonesia and strong negative CO anomaly over South America at 215 hPa (Fig. 13). In all three events, positive precipitation anomalies occurred over the central Pacific, consistent with the positive 215 hPa IWC anomalies discussed before. During La Niña periods, CO emission generally shows opposite anomalies over Indonesia, Australia and South America against El Niño periods. Precipitation also shows opposite anomalies over the central Pacific. However, both CO emission and precipitation anomalies do not show clear difference between different ENSO types over the African continent.

To investigate the differences of CO transport pathways between different ENSO types, we performed analysis using the pathway auto-identification method developed in Huang et al. (2012). Since CloudSat was launched in 2006, here we only have two El Niño years (2006 and 2009) and two La Niña years (2007 and 2010) for the analysis. First, we calculate the relative frequency of each transport pathway, which is defined as the percentage of CO increase cases associated with each pathway normalized by the total number of CO increase cases within each 4° latitude \times 8° longitude grid box. The results are shown in Figs. 15 and 16, for the “local convection” and the “LT advection \rightarrow convection” pathway, respectively. The “local convection” pathway occurred more frequently over South America than over southern Africa, while the frequency was lowest over the Indonesian region (Fig. 15). Although the UT CO concentration over South America was much higher in 2006 than that in 2009 (Fig. 13), the frequency of “local convection” pathway did not show much difference. Similarly, the frequency of “local convection” pathway was larger in 2007 than that in 2010 over South America, but the UT CO was higher in 2010. Thus, the interannual variation of the frequency of “local convection” pathway appeared to be not consistent with the IAV of UT CO over South America and this conclusion also applied to other tropical continents. Besides, the fre-

Impacts of fire emissions and transport pathways

L. Huang et al.

Title Page

Abstract

Introduction

Conclusions

References

Tables

Figures



Back

Close

Full Screen / Esc

Printer-friendly Version

Interactive Discussion



Impacts of fire emissions and transport pathways

L. Huang et al.

Title Page

Abstract

Introduction

Conclusions

References

Tables

Figures

◀

▶

◀

▶

Back

Close

Full Screen / Esc

Printer-friendly Version

Interactive Discussion



quency of “local convection” pathway did not show clear difference between different ENSO types. For the “LT advection → convection” pathway, it occurred more frequently over maritime areas than over continents, especially over the tropical western Pacific and northern Indian Ocean (Fig. 16). The frequency of “LT advection → convection” pathway appeared to be higher over the west-central Pacific (near Indonesia) during El Niño years than during La Niña years, which may account for the UT CO differences over this region between different ENSO types (Fig. 13).

Second, we calculate the average increase of CO concentration at 215 hPa associated with the “local convection” and the “LT advection → convection” pathway, and the results are shown in Figs. 17 and 18, respectively. In general, the interannual variation of average CO increase associated with the “local convection” pathway is consistent with the IAV of UT CO over the tropical continents (Fig. 17). For example, the higher CO concentrations over South America during 2006 than 2009 (both are El Niño years), or during 2010 than 2007 (both are La Niña years), were corresponding to the higher average CO increase associated with the “local convection” pathway during that year. Besides, the average CO increase associated with the “local convection” pathway appeared to be higher over Indonesia-Australia and lower over South America during El Niño years than those during La Niña years, which indicates clear differences of CO transport between different ENSO types. The average CO increase associated with the “LT advection → convection” pathway was higher over the Indonesian region during 2006 and over the southern South America (15–30° S) during 2010, compared with other years (Fig. 18). Except these two regions, the interannual variation was small. The average CO increase associated with the “LT advection → convection” pathway did not show clear difference between different ENSO types over the tropics.

To quantify the differences of CO transport from the surface to the UT between two different El Niño types (2006 and 2009), we choose three tropical land regions, South America (24° S–12° N, 88–32° W), Central Africa (20° S–20° N, 16° W–40° E) and Indonesia (10° S–10° N, 90° E–160° E), since they represent the main CO source regions and/or UT CO centers. The results are shown in Table 5. Over Central Africa, although

Impacts of fire emissions and transport pathways

L. Huang et al.

Title Page

Abstract

Introduction

Conclusions

References

Tables

Figures

◀

▶

◀

▶

Back

Close

Full Screen / Esc

Printer-friendly Version

Interactive Discussion



the number of “local convection” events was smaller in 2006 than that in 2009, the number of “LT advection → convection” events was larger, thus the total number of transport events was nearly equal between the two years. In addition, the average CO increase associated with either pathway was also comparable between 2006 and 2009. Thus, the overall CO transport over this region did not show much difference between the two years. Over South America, the number of “LT advection → convection” events was much larger in 2006 than that in 2009, while the number of “local convection” events was nearly equal. However, the average CO increase (ΔCO) associated with “local convection” was significantly lower in 2009 (58.6 ppbv) than that in 2006 (75.5 ppbv), while ΔCO associated with “LT advection → convection” was nearly equal. This may be the reason for the strong negative UT CO anomaly in 2009 over this region. Over Indonesia, the numbers of both pathway events were larger in 2009 than those in 2006, despite the fact that stronger positive UT CO anomaly occurred in 2006. To explain this “paradox”, we again checked ΔCO associated with each pathway. Indeed, the average CO increase associated with “local convection” was significantly higher in 2006 (73.8 ppbv) than that in 2009 (47.8 ppbv). In addition, ΔCO associated with “LT advection → convection” pathway was also higher in 2006, but the difference between the two years was much less. The reason why fewer transport events were identified in 2006 than 2009 over Indonesia may be due to higher background CO concentrations in the UT which are used to determine CO changes for identifying transport pathways.

6 Conclusions

In this study, we have identified the dominant modes of the interannual variation of tropical UT CO by using rotated EOF analysis, and evaluated the field relationships between SST, convection, CO emission and UT CO interannual variation by using SVD analysis. The differences of CO emission, convection and transport pathways between different ENSO types are investigated by using satellite observation data and pathway

auto-identification method developed in our previous study. The main conclusions are summarized as follows:

Indonesia is the most significant tropical land region that affects UT CO interannual variation, as suggested by the first REOF mode of UT CO. ENSO is the dominant climate condition affecting the time evolution of the first REOF mode. The second REOF mode identified a strong center over South America, and indicated the significant influence of the Atlantic Ocean SST. The third REOF mode identified a strong center over West Africa and tropical Atlantic Ocean, and the time evolution of this REOF mode appears to be affected by various climate conditions.

Over South America, the IAV of UT CO is mainly affected by the IAV of surface CO emission, as suggested by the significant correlation between the monthly anomalies of UT CO and CO emission. Over Central Africa, CO emission has little impact on the IAV of UT CO, while convective transport may play an important role. Over SE Asia, both CO emission and convective transport are important in determining the IAV of UT CO. Over the whole Tropics, the IAV of UT CO is mainly affected by the IAV of CO emission, which is similar to that over South America.

The SVD analyses suggest that ENSO is the dominant climate condition that affects the field relationships between UT CO and SST, UT CO and convection, as well as UT CO and CO emission. The variation of convection is closely related to the SST changes as suggested by the similarity between SVD analyses of CO-SST and CO-IWC. AMO appears to have significant impact on the field relationship between UT CO and CO emission, probably through its impact on the rainfall in South America and Africa (Knight et al., 2006).

The impacts of different ENSO types on the IAV of CO in the tropical UT are analyzed through two ways: factor analysis and transport pathway analysis. During boreal fall season, UT CO shows positive anomalies over the Indonesian region and Indian Ocean in El Niño years, compared to negative anomalies over the same region in La Niña years. This is closely related to the in-phase CO emission anomalies. UT CO shows consistently strong positive anomalies over South America in La Niña

Impacts of fire emissions and transport pathways

L. Huang et al.

Title Page

Abstract

Introduction

Conclusions

References

Tables

Figures

◀

▶

◀

▶

Back

Close

Full Screen / Esc

Printer-friendly Version

Interactive Discussion



years, which is associated with positive CO emission anomalies. Over the central Pacific (around the dateline), positive (negative) UT CO anomalies occurs in El Niño (La Niña) years, mainly due to positive (negative) convection anomalies.

Through the transport pathway analysis, we found that the IAV of UT CO over the tropical continents is consistent with that of the average CO increase associated with the “local convection” pathway, instead of the relative frequency of this pathway. The relative frequency of the “LT advection → convection” pathway appears to be the factor that accounts for the UT CO differences over the west-central Pacific between different ENSO types. Besides, different ENSO types have different impacts on the average CO transported by the “local convection” pathway, which appears to be higher over Indonesia-Australia and lower over South America during El Niño years than that during La Niña years. Although both 2006 and 2009 are El Niño years, the ENSO types are totally different, as demonstrated by the SST anomaly pattern. The results of transport pathway analysis suggest that the average CO transported per event of “local convection”, instead of the number of transport events, is the factor that accounts for the UT CO difference between these two El Niño periods over South America and Indonesia. The contribution from the difference of “LT advection → convection” pathway is much smaller and negligible compared to the “local convection” pathway.

Although previous studies have found that ENSO has significant impact on the IAV of UT CO (e.g., Edwards et al., 2006b; Duncan and Logan, 2008), this work is consistent with previous findings by directly evaluating the UT CO anomaly field. Besides, we found that different ENSO types have rather different impacts on spatial pattern of the UT CO, which is related to the differences in CO transport. Although we have analyzed the impacts of different ENSO types on the IAV of tropical UT CO, due to the limited satellite observations, we only have a relatively short period of data for the transport pathway analysis; whether the characteristics and differences apply to other ENSO years still need further studies. Both EOF and SVD analyses have identified other climate indices (e.g., PDO, AMO) as secondary factors affecting the interannual

Impacts of fire emissions and transport pathways

L. Huang et al.

[Title Page](#)[Abstract](#)[Introduction](#)[Conclusions](#)[References](#)[Tables](#)[Figures](#)[Back](#)[Close](#)[Full Screen / Esc](#)[Printer-friendly Version](#)[Interactive Discussion](#)

variation of UT CO, but the mechanisms are still not clear. These questions will need to be addressed in future studies.

Acknowledgements. This research is supported by the NASA Aura Science Team (AST) program (NNX09AD85G), the Jackson School of Geosciences at the University of Texas at Austin, and the Jet Propulsion Laboratory, California Institute of Technology, under contract with NASA. We acknowledge the NASA CloudSat project for the CloudSat data.

References

- Adler, R. F., Huffman, G. J., Chang, A., Ferraro, R., Xie, P. P., Janowiak, J., Rudolf, B., Schneider, U., Curtis, S., and Bolvin, D.: The version-2 global precipitation climatology project (GPCP) monthly precipitation analysis (1979–present), *J. Hydrometeorol.*, 4, 1147–1167, 2003.
- Andreae, M. O., Artaxo, P., Fischer, H., Freitas, S. R., Gregoire, J. M., Hansel, A., Hoor, P., Kormann, R., Krejci, R., Lange, L., Lelieveld, J., Lindinger, W., Longo, K., Peters, W., de Reus, M., Scheeren, B., Dias, M. A. F. S., Strom, J., van Velthoven, P. F. J., and Williams, J.: Transport of biomass burning smoke to the upper troposphere by deep convection in the equatorial region, *Geophys. Res. Lett.*, 28, 951–954, 2001.
- Andreae, M. O., Rosenfeld, D., Artaxo, P., Costa, A. A., Frank, G. P., Longo, K. M., and Silva-Dias, M. A. F.: Smoking rain clouds over the Amazon, *Science*, 303, 1337–1342, 2004.
- Ashok, K., Behera, S. K., Rao, S. A., Weng, H., and Yamagata, T.: El Niño Modoki and its possible teleconnection, *J. Geophys. Res.*, 112, C11007, doi:10.1029/2006jc003798, 2007.
- Bretherton, C. S., Widmann, M., Dymnikov, V. P., Wallace, J. M., and Bladé, I.: The effective number of spatial degrees of freedom of a time-varying field, *J. Climate*, 12, 1990–2009, 1999.
- Chandra, S., Ziemke, J. R., Duncan, B. N., Diehl, T. L., Livesey, N. J., and Froidevaux, L.: Effects of the 2006 El Niño on tropospheric ozone and carbon monoxide: implications for dynamics and biomass burning, *Atmos. Chem. Phys.*, 9, 4239–4249, doi:10.5194/acp-9-4239-2009, 2009.
- CloudSat Project: CloudSat Standard Data Products Handbook, Cooperative Institutes for Research in the Atmosphere, Colorado State University, Fort Collins, CO, 2008.

Impacts of fire emissions and transport pathways

L. Huang et al.

Title Page

Abstract

Introduction

Conclusions

References

Tables

Figures

◀

▶

◀

▶

Back

Close

Full Screen / Esc

Printer-friendly Version

Interactive Discussion



Impacts of fire emissions and transport pathways

L. Huang et al.

Title Page

Abstract

Introduction

Conclusions

References

Tables

Figures

◀

▶

◀

▶

Back

Close

Full Screen / Esc

Printer-friendly Version

Interactive Discussion

- Daniel, J. S. and Solomon, S.: On the climate forcing of carbon monoxide, *J. Geophys. Res.*, 103, 13249–13260, 1998.
- Duncan, B. N. and Logan, J. A.: Model analysis of the factors regulating the trends and variability of carbon monoxide between 1988 and 1997, *Atmos. Chem. Phys.*, 8, 7389–7403, doi:10.5194/acp-8-7389-2008, 2008.
- 5 Duncan, B. N., Strahan, S. E., Yoshida, Y., Steenrod, S. D., and Livesey, N.: Model study of the cross-tropopause transport of biomass burning pollution, *Atmos. Chem. Phys.*, 7, 3713–3736, doi:10.5194/acp-7-3713-2007, 2007.
- Edwards, D. P., Emmons, L. K., Gille, J. C., Chu, A., Attie, J. L., Giglio, L., Wood, S. W., Haywood, J., Deeter, M. N., Massie, S. T., Ziskin, D. C., and Drummond, J. R.: Satellite-observed pollution from Southern Hemisphere biomass burning, *J. Geophys. Res.-Atmos.*, 111, D14312, doi:10.1029/2005jd006655, 2006a.
- 10 Edwards, D. P., Petron, G., Novelli, P. C., Emmons, L. K., Gille, J. C., and Drummond, J. R.: Southern Hemisphere carbon monoxide interannual variability observed by Terra/Measurement of Pollution in the Troposphere (MOPITT), *J. Geophys. Res.-Atmos.*, 111, D16303, doi:10.1029/2006jd007079, 2006b.
- Enfield, D. B. and Mestas-Núñez, A. M.: *El Niño and Southern Oscillation: Multi-Scale Variability and Global and Regional Impacts*, edited by: Henry, F., Diaz and Vera Markgraf, Cambridge University Press, 2000.
- 20 Folkins, I., Chatfield, R., Baumgardner, D., and Proffitt, M.: Biomass burning and deep convection in southeastern Asia: results from ASHOE/MAESA, *J. Geophys. Res.-Atmos.*, 102, 13291–13299, 1997.
- Giglio, L., van der Werf, G. R., Randerson, J. T., Collatz, G. J., and Kasibhatla, P.: Global estimation of burned area using MODIS active fire observations, *Atmos. Chem. Phys.*, 6, 957–974, doi:10.5194/acp-6-957-2006, 2006.
- 25 Giglio, L., Randerson, J. T., van der Werf, G. R., Kasibhatla, P. S., Collatz, G. J., Morton, D. C., and DeFries, R. S.: Assessing variability and long-term trends in burned area by merging multiple satellite fire products, *Biogeosciences*, 7, 1171–1186, doi:10.5194/bg-7-1171-2010, 2010.
- 30 Gonzi, S. and Palmer, P. I.: Vertical transport of surface fire emissions observed from space, *J. Geophys. Res.*, 115, D02306, doi:10.1029/2009JD012053, 2010.

Impacts of fire emissions and transport pathways

L. Huang et al.

Title Page

Abstract

Introduction

Conclusions

References

Tables

Figures

◀

▶

◀

▶

Back

Close

Full Screen / Esc

Printer-friendly Version

Interactive Discussion



Huang, L., Fu, R., Jiang, J. H., Wright, J. S., and Luo, M.: Geographic and seasonal distributions of CO transport pathways and their roles in determining CO centers in the upper troposphere, *Atmos. Chem. Phys.*, 12, 4683–4698, doi:10.5194/acp-12-4683-2012, 2012.

Jiang, J. H., Livesey, N. J., Su, H., Neary, L., McConnell, J. C., and Richards, N. A. D.: Connecting surface emissions, convective uplifting, and long-range transport of carbon monoxide in the upper troposphere: new observations from the Aura Microwave Limb Sounder, *Geophys. Res. Lett.*, 34, L18812, doi:10.1029/2007gl030638, 2007.

Jiang, J. H., Su, H., Zhai, C., Massie, S. T., Schoeberl, M. R., Colarco, P. R., Platnick, S., Gu, Y., and Liou, K.-N.: Influence of convection and aerosol pollution on ice cloud particle effective radius, *Atmos. Chem. Phys.*, 11, 457–463, doi:10.5194/acp-11-457-2011, 2011.

Kao, H. Y. and Yu, J. Y.: Contrasting eastern-Pacific and central-Pacific types of ENSO, *J. Climate*, 22, 615–632, 2009.

Knight, J. R., Folland, C. K., and Scaife, A. A.: Climate impacts of the Atlantic multidecadal oscillation, *Geophys. Res. Lett.*, 33, L17706, doi:10.1029/2006GL026242, 2006.

Kug, J. S., Jin, F. F., and An, S. I.: Two Types of El Niño Events: cold tongue El Niño and warm pool El Niño, *J. Climate*, 22, 1499–1515, doi:10.1175/2008jcli2624.1, 2009.

Lee, T., Hobbs, W. R., Willis, J. K., Halkides, D., Fukumori, I., Armstrong, E. M., Hayashi, A. K., Liu, W. T., Patzert, W., and Wang, O.: Record warming in the South Pacific and western Antarctica associated with the strong central-Pacific El Niño in 2009–10, *Geophys. Res. Lett.*, 37, L19704, doi:10.1029/2010gl044865, 2010.

Liu, C. T., Zipser, E., Garrett, T., Jiang, J. H., and Su, H.: How do the water vapor and carbon monoxide “tape recorders” start near the tropical tropopause?, *Geophys. Res. Lett.*, 34, L09804, doi:10.1029/2006gl029234, 2007.

Junhua Liu, Logan, J. A., Jones, D. B. A., Livesey, N. J., Megretskaia, I., Carouge, C., and Nedelec, P.: Analysis of CO in the tropical troposphere using Aura satellite data and the GEOS-Chem model: insights into transport characteristics of the GEOS meteorological products, *Atmos. Chem. Phys.*, 10, 12207–12232, doi:10.5194/acp-10-12207-2010, 2010.

Liu, J., Logan, J. A., Murray, L. T., Pumphrey, H. C., Schwartz, M. J., and Megretskaia, I. A.: Transport analysis and source attribution of seasonal and interannual variability of CO in the tropical upper troposphere and lower stratosphere, *Atmos. Chem. Phys.*, 13, 129–146, doi:10.5194/acp-13-129-2013, 2013.

Livesey, R. E. and Chen, W. Y.: Statistical field significance and its determination by Monte Carlo techniques, *Mon. Weather Rev.*, 111, 46–59, 1983.

Impacts of fire emissions and transport pathways

L. Huang et al.

Title Page

Abstract

Introduction

Conclusions

References

Tables

Figures

◀

▶

◀

▶

Back

Close

Full Screen / Esc

Printer-friendly Version

Interactive Discussion



- Livesey, N. J., Filipiak, M. J., Froidevaux, L., Read, W. G., Lambert, A., Santee, M. L., Jiang, J. H., Pumphrey, H. C., Waters, J. W., Cofield, R. E., Cuddy, D. T., Daffer, W. H., Drouin, B. J., Fuller, R. A., Jarnot, R. F., Jiang, Y. B., Knosp, B. W., Li, Q. B., Perun, V. S., Schwartz, M. J., Snyder, W. V., Stek, P. C., Thurstans, R. P., Wagner, P. A., Avery, M., Brownell, E. V., Cammas, J. P., Christensen, L. E., Diskin, G. S., Gao, R. S., Jost, H. J., Loewenstein, M., Lopez, J. D., Nedelec, P., Osterman, G. B., Sachse, G. W., and Webster, C. R.: Validation of Aura Microwave Limb Sounder O₃ and CO observations in the upper troposphere and lower stratosphere, *J. Geophys. Res.-Atmos.*, 113, D15S02, doi:10.1029/2007jd008805, 2008.
- Livesey, N. J., Read, W. G., Froidevaux, L., Lambert, A., and Manney, G. L.: EOS MLS Version 3.3 Level 2 Data Quality and Description Document, Jet Propulsion Laboratory, California Institute of Technology, Pasadena, CA, 2011.
- Livesey, N. J., Logan, J. A., Santee, M. L., Waters, J. W., Doherty, R. M., Read, W. G., Froidevaux, L., and Jiang, J. H.: Interrelated variations of O₃, CO and deep convection in the tropical/subtropical upper troposphere observed by the Aura Microwave Limb Sounder (MLS) during 2004–2011, *Atmos. Chem. Phys.*, 13, 579–598, doi:10.5194/acp-13-579-2013, 2013.
- Logan, J. A., Megretskaia, I., Nassar, R., Murray, L. T., Zhang, L., Bowman, K. W., Worden, H. M., and Luo, M.: Effects of the 2006 El Niño on tropospheric composition as revealed by data from the Tropospheric Emission Spectrometer (TES), *Geophys. Res. Lett.*, 35, L03816, doi:10.1029/2007GL031698, 2008.
- Lorenz, E. N.: Empirical orthogonal functions and statistical weather prediction, Technical report, Statistical Forecast Project Report 1, Dept. of Meteor., MIT, 49 pp., 1956.
- Mu, M., Randerson, J. T., van der Werf, G. R., Giglio, L., Kasibhatla, P., Morton, D., Collatz, G. J., DeFries, R. S., Hyer, E. J., Prins, E. M., Griffith, D. W. T., Wunch, D., Toon, G. C., Sherlock, V., and Wennberg, P. O.: Daily and 3-hourly variability in global fire emissions and consequences for atmospheric model predictions of carbon monoxide, *J. Geophys. Res.-Atmos.*, 116, doi:10.1029/2011jd016245, 2011.
- North, G. R., Bell, T. L., Cahalan, R. F., and Moeng, F. J.: Sampling errors in the estimation of empirical orthogonal functions, *Mon. Weather Rev.*, 110, 699–706, 1982.
- Novelli, P., Masarie, K., and Lang, P.: Distributions and recent changes of carbon monoxide in the lower troposphere, *J. Geophys. Res.*, 103, 19015–19033, 1998.
- Pickering, K. E., Thompson, A. M., Wang, Y. S., Tao, W. K., McNamara, D. P., Kirchoff, V. W. J. H., Heikes, B. G., Sachse, G. W., Bradshaw, J. D., Gregory, G. L., and

Impacts of fire emissions and transport pathways

L. Huang et al.

Title Page

Abstract

Introduction

Conclusions

References

Tables

Figures

◀

▶

◀

▶

Back

Close

Full Screen / Esc

Printer-friendly Version

Interactive Discussion



Blake, D. R.: Convective transport of biomass burning emissions over Brazil during TRACE A, *J. Geophys. Res.-Atmos.*, 101, 23993–24012, 1996.

Reynolds, R. W., Rayner, N. A., Smith, T. M., Stokes, D. C., and Wang, W.: An improved in situ and satellite SST analysis for climate, *J. Climate*, 15, 1609–1625, 2002.

5 Ricaud, P., Barret, B., Attié, J.-L., Motte, E., Le Flochmoën, E., Teysseïre, H., Peuch, V.-H., Livesey, N., Lambert, A., and Pommereau, J.-P.: Impact of land convection on troposphere-stratosphere exchange in the tropics, *Atmos. Chem. Phys.*, 7, 5639–5657, doi:10.5194/acp-7-5639-2007, 2007.

10 Richman, M. B.: Rotation of principal components, *J. Climatol.*, 6, 293–335, doi:10.1002/joc.3370060305, 1986.

Schoeberl, M. R., Duncan, B. N., Douglass, A. R., Waters, J., Livesey, N., Read, W., and Filipiak, M.: The carbon monoxide tape recorder, *Geophys. Res. Lett.*, 33, L12811, doi:10.1029/2006gl026178, 2006.

15 Stephens, G. L., Vane, D. G., Boain, R. J., Mace, G. G., Sassen, K., Wang, Z. E., Illingworth, A. J., O'Connor, E. J., Rossow, W. B., Durden, S. L., Miller, S. D., Austin, R. T., Benedetti, A., Mitrescu, C., and Team, C. S.: The cloudsat mission and the a-train – a new dimension of space-based observations of clouds and precipitation, *B. Am. Meteorol. Soc.*, 83, 1771–1790, doi:10.1175/Bams-83-12-1771, 2002.

20 Su, H. and Jiang, J. H.: Tropical clouds and circulation changes during the 2006/07 and 2009/10 El Niños, *J. Climate*, 26, 399–413, doi:10.1175/JCLI-D-12-00152.1, 2013.

Thompson, A. M.: The oxidizing capacity of the earth's atmosphere: probable past and future changes, *Science*, 256, 1157, 1157–1165, doi:10.1126/science.256.5060.1157, 1992.

25 Thompson, A. M., Pickering, K. E., McNamara, D. P., Schoeberl, M. R., Hudson, R. D., Kim, J. H., Browell, E. V., Kirchhoff, V. W. J. H., and Nganga, D.: Where did tropospheric ozone over southern Africa and the tropical Atlantic come from in October 1992? Insights from TOMS, GTE TRACE A, and SAFARI 1992, *J. Geophys. Res.-Atmos.*, 101, 24251–24278, 1996.

van der Werf, G. R., Randerson, J. T., Giglio, L., Collatz, G. J., Mu, M., Kasibhatla, P. S., Morton, D. C., DeFries, R. S., Jin, Y., and van Leeuwen, T. T.: Global fire emissions and the contribution of deforestation, savanna, forest, agricultural, and peat fires (1997–2009), *Atmos. Chem. Phys.*, 10, 11707–11735, doi:10.5194/acp-10-11707-2010, 2010.

30 Wallace, J., Smith, C., and Bretherton, C.: Singular value decomposition of wintertime sea surface temperature and 500-mb height anomalies, *J. Climate*, 5, 561–576, 1992.

Impacts of fire emissions and transport pathways

L. Huang et al.

Title Page

Abstract

Introduction

Conclusions

References

Tables

Figures

◀

▶

◀

▶

Back

Close

Full Screen / Esc

Printer-friendly Version

Interactive Discussion



Waters, J. W., Froidevaux, L., Harwood, R. S., Jarnot, R. F., Pickett, H. M., Read, W. G., Siegel, P. H., Cofield, R. E., Filipiak, M. J., Flower, D. A., Holden, J. R., Lau, G. K., Livesey, N. J., Manney, G. L., Pumphrey, H. C., Santee, M. L., Wu, D. L., Cuddy, D. T., Lay, R. R., Loo, M. S., Perun, V. S., Schwartz, M. J., Stek, P. C., Thurstans, R. P., Chandra, K. M., Chavez, M. C., Chen, G., Boyles, M. A., Chudasama, B. V., Dodge, R., Fuller, R. A., Girard, M. A., Jiang, J. H., Jiang, Y., Knosp, B. W., LaBelle, R. C., Lam, J. C., Lee, K. A., Miller, D., Oswald, J. E., Patel, N. C., Pukala, D. M., Quintero, O., Scaff, D. M., Snyder, W. V., Tope, M. C., Wagner, P. A., and Walch, M. J.: The Earth Observing System Microwave Limb Sounder (EOS MLS) on the Aura satellite, *IEEE T. Geosci. Remote*, 44, 1075–1092, 2006.

Wotawa, G., Novelli, P., Trainer, M., and Granier, C.: Inter-annual variability of summertime CO concentrations in the Northern Hemisphere explained by boreal forest fires in North America and Russia, *Geophys. Res. Lett.*, 28, 4575–4578, 2001.

Wu, D. L., Jiang, J. H., Read, W. G., Austin, R. T., David, C. P., Lambert, A., Stephens, G. L., Vane, D. G., and Waters, J. W.: Validation of Aura MLS cloud Ice Water Content (IWC) measurements, *J. Geophys. Res.*, 113, D15S10, doi:10.1029/2007JD008931, 2008.

Yeh, S. W., Kug, J. S., Dewitte, B., Kwon, M. H., Kirtman, B. P., and Jin, F. F.: El Niño in a changing climate, *Nature*, 461, 511–514, doi:10.1038/Nature08316, 2009.

Impacts of fire emissions and transport pathways

L. Huang et al.

Table 1. Correlation coefficients between the rotated principle components (PCs) of the first three REOF modes of 147 hPa CO and 16 climate indices. The values that are significant at the 90 % confidence level after considering autocorrelation are shown in bold. The acronyms represent (from left to right): Atlantic Meridional Mode (AMM), Atlantic Multidecadal Oscillation (AMO), East Pacific/North Pacific Oscillation (EP/NP), North Atlantic Oscillation (NAO), Pacific Decadal Oscillation (PDO), Pacific North American Index (PNA), Quasi-Biennial Oscillation (QBO), Southern Oscillation Index (SOI), Tropical Northern Atlantic Index (TNA), Tropical Southern Atlantic Index (TSA), Western Pacific Index (WP), Arctic Oscillation (AO) and Dipole Mode Index (DMI).

	amm	amo	ep/np	nao	nino3	nino4	nino3.4	pdo	pna	qbo	soi	tna	tsa	wp	ao	dmi
CO	0.008	-0.158	-0.13	0.045	-0.251	-0.356	-0.301	-0.229	0.197	-0.305	0.321	-0.058	-0.008	-0.018	-0.075	-0.283
PC1																
CO	0.254	0.361	-0.102	-0.219	-0.048	-0.069	-0.067	0.004	0.172	0.017	0.116	0.277	0.087	0.113	-0.078	-0.053
PC2																
CO	-0.09	-0.057	-0.053	0.158	-0.172	-0.388	-0.359	-0.334	-0.352	0.335	0.284	-0.189	0.107	-0.296	0.283	-0.145
PC3																

Title Page

Abstract

Introduction

Conclusions

References

Tables

Figures

◀

▶

◀

▶

Back

Close

Full Screen / Esc

Printer-friendly Version

Interactive Discussion



Impacts of fire emissions and transport pathways

L. Huang et al.

Table 2. Correlation coefficients between 16 climate indices and the principle components (PCs) of the first three SVD modes of 147 hPa CO and SST. The values that are significant at the 90 % confidence level after considering autocorrelation are shown in bold.

	amm	amo	ep/np	nao	nino3	nino4	nino3.4	pdo	pna	qbo	soi	tna	tsa	wp	ao	dmi
CO mode 1	0.003	0.174	0.165	-0.056	0.343	0.527	0.456	0.395	-0.073	0.12	-0.485	0.108	-0.03	0.017	-0.005	0.277
SST mode 1	-0.066	0.142	0.125	-0.118	0.575	0.872	0.815	0.554	0.068	-0.058	-0.763	0.21	0.038	0.05	-0.154	0.267
CO mode 2	-0.143	-0.299	-0.021	0.041	0.024	0.029	0.077	0.014	0.122	-0.29	0.033	-0.11	-0.068	0.136	-0.153	-0.068
SST mode 2	-0.121	-0.106	0.079	-0.128	0.295	0.509	0.499	0.342	0.237	-0.361	-0.421	0.056	0.013	0.173	-0.293	0.139
CO mode 3	0.44	0.449	-0.061	-0.276	0	0.097	0.072	0.18	0.327	-0.201	-0.037	0.499	0.041	0.051	-0.222	0.033
SST mode 3	0.605	0.557	-0.022	-0.304	0.068	0.329	0.246	0.424	0.364	-0.448	-0.18	0.755	0.11	-0.007	-0.388	0.152

Title Page

Abstract

Introduction

Conclusions

References

Tables

Figures

◀

▶

◀

▶

Back

Close

Full Screen / Esc

Printer-friendly Version

Interactive Discussion



Impacts of fire emissions and transport pathways

L. Huang et al.

Table 3. As in Table 2, but for 147 hPa CO and 215 hPa IWC.

	amm	amo	ep/np	nao	nino3	nino4	nino3.4	pdo	pna	qbo	soi	tna	tsa	wp	ao	dmi
CO mode 1	0.005	0.178	0.165	-0.051	0.326	0.504	0.431	0.38	-0.085	0.139	-0.477	0.101	-0.026	0.007	0.008	0.268
IWC mode 1	-0.04	0.124	0.083	-0.103	0.494	0.799	0.728	0.542	0.066	-0.127	-0.775	0.182	0.012	0.114	-0.156	0.256
CO mode 2	0.159	0.304	0.007	-0.063	-0.039	-0.055	-0.097	-0.029	-0.12	0.305	-0.004	0.125	0.083	-0.13	0.135	0.058
IWC mode 2	0.012	0.004	0.043	-0.036	-0.234	-0.436	-0.409	-0.293	-0.295	0.407	0.375	-0.093	0.215	-0.182	0.135	0.018
CO mode 3	0.384	0.41	-0.073	-0.236	-0.006	0.138	0.088	0.196	0.34	-0.27	-0.132	0.43	0.002	0.028	-0.214	-0.043
IWC mode 3	0.237	0.3	-0.153	-0.139	0.161	0.447	0.364	0.369	0.322	-0.328	-0.47	0.37	-0.025	-0.025	-0.24	0.021

Title Page

Abstract

Introduction

Conclusions

References

Tables

Figures

⏪

⏩

◀

▶

Back

Close

Full Screen / Esc

Printer-friendly Version

Interactive Discussion



Impacts of fire emissions and transport pathways

L. Huang et al.

Table 4. As in Table 2, but for 147 hPa CO and surface CO emission.

	amm	amo	ep/np	nao	nino3	nino4	nino3.4	pdo	pna	qbo	soi	tna	tsa	wp	ao	dmi
CO	0.014	-0.165	-0.16	0.037	-0.277	-0.403	-0.339	-0.291	0.167	-0.244	0.4	-0.057	0.003	0.025	-0.06	-0.255
mode 1																
CO_emi	0.035	-0.103	-0.264	0.209	-0.209	-0.266	-0.233	-0.152	0.25	-0.194	0.304	-0.061	0.016	0.018	0.063	-0.26
mode 1																
CO	0.359	0.449	0.001	-0.226	0.004	0.005	-0.006	0.07	0.111	0.088	0.066	0.38	0.064	0.064	-0.041	0.212
mode 2																
CO_emi	0.142	0.253	-0.036	-0.105	-0.148	-0.147	-0.181	-0.012	0.041	-0.078	0.105	0.114	0.01	0.146	-0.033	0.121
mode 2																
CO	-0.107	-0.244	0.016	0.009	0.1	0.078	0.142	0.038	0.078	-0.196	0.038	-0.04	-0.046	0.158	-0.137	0.087
mode 3																
CO_emi	0.081	-0.019	-0.012	-0.054	0.121	0.082	0.124	-0.065	0.042	0.002	-0.018	0.177	0.085	0.077	-0.024	0.446
mode 3																

Title Page

Abstract

Introduction

Conclusions

References

Tables

Figures

⏪

⏩

◀

▶

Back

Close

Full Screen / Esc

Printer-friendly Version

Interactive Discussion



Impacts of fire emissions and transport pathways

L. Huang et al.

Title Page

Abstract

Introduction

Conclusions

References

Tables

Figures



Back

Close

Full Screen / Esc

Printer-friendly Version

Interactive Discussion



Table 5. Results of CO transport pathway analyses over Central Africa (AF), South America (SA) and Indonesia (IN). From left to right, the 1st column indicates the regions, the 2nd and 7th columns indicate the number of “local convection” events, the 3rd and 8th columns indicate average CO increase (ppbv) associated with “local convection” pathway, the 4th and 9th columns indicate the number of “LT advection → convection” events, the 5th and 10th columns indicate average CO increase (ppbv) associated with “LT advection → convection” pathway, the 6th and 11th columns indicate the total number of CO transport events during SON in each year.

	loc-conv		2006 SON		total	loc-conv		2009 SON		total
	num of events	ΔCO	LT adv-conv num of events	ΔCO		num of events	num of events	ΔCO	LT adv-conv num of events	
AF	81	59.88	240	43.52	321	104	53.61	199	47.5	303
SA	154	75.46	358	51.59	512	157	58.6	319	53.23	476
IN	32	73.78	281	53.23	313	43	47.78	344	46.07	387

Impacts of fire emissions and transport pathways

L. Huang et al.

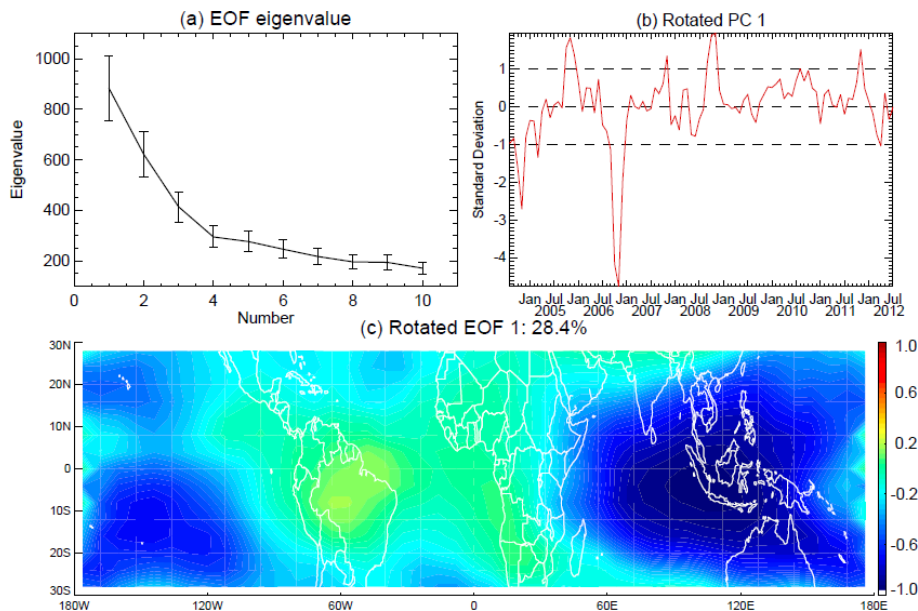


Fig. 1. (a) The first 10 EOF eigenvalues; (b) the first rotated principle component; (c) spatial pattern of the first rotated REOF mode of monthly anomalies of CO at 147 hPa for the period of August 2004–July 2012. The error bars in (a) represent the uncertainties of each eigenvalue based on a “rule of thumb” (North et al., 1982). The dash lines in (b) indicate 0 and ± 1 standard deviations. The spatial pattern in (c) is shown as homogeneous correlation map.

Impacts of fire emissions and transport pathways

L. Huang et al.

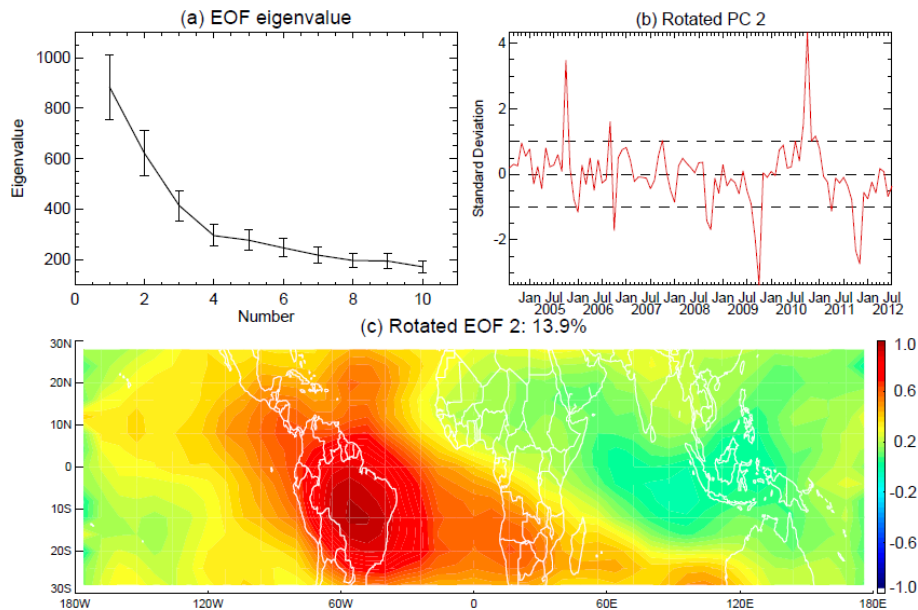


Fig. 2. As in Fig. 1, but for the second REOF mode of CO at 147 hPa.

[Title Page](#)[Abstract](#)[Introduction](#)[Conclusions](#)[References](#)[Tables](#)[Figures](#)[◀](#)[▶](#)[◀](#)[▶](#)[Back](#)[Close](#)[Full Screen / Esc](#)[Printer-friendly Version](#)[Interactive Discussion](#)

Impacts of fire emissions and transport pathways

L. Huang et al.

Title Page

Abstract

Introduction

Conclusions

References

Tables

Figures

◀

▶

◀

▶

Back

Close

Full Screen / Esc

Printer-friendly Version

Interactive Discussion

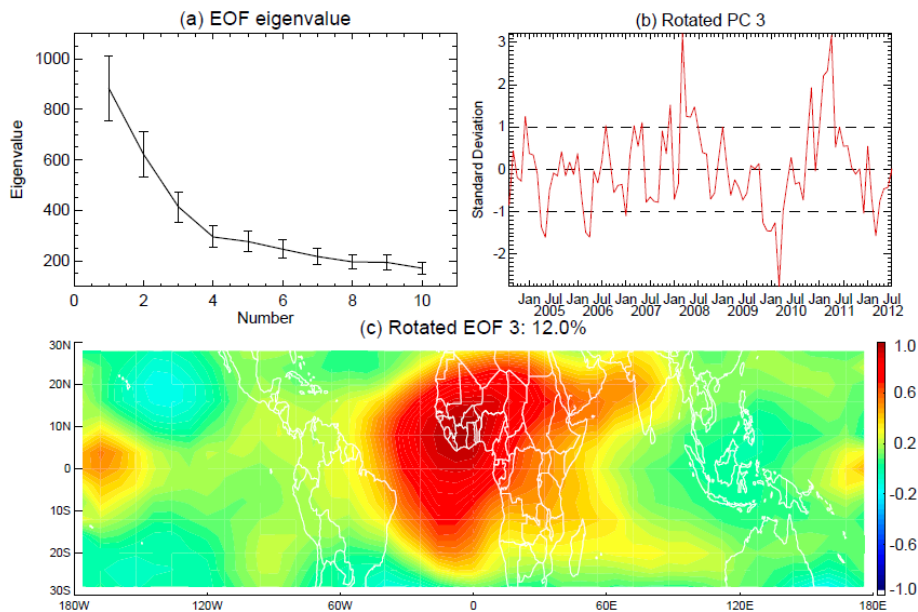


Fig. 3. As in Fig. 1, but for the third REOF mode of CO at 147 hPa.

Impacts of fire emissions and transport pathways

L. Huang et al.

Title Page

Abstract

Introduction

Conclusions

References

Tables

Figures

◀

▶

◀

▶

Back

Close

Full Screen / Esc

Printer-friendly Version

Interactive Discussion

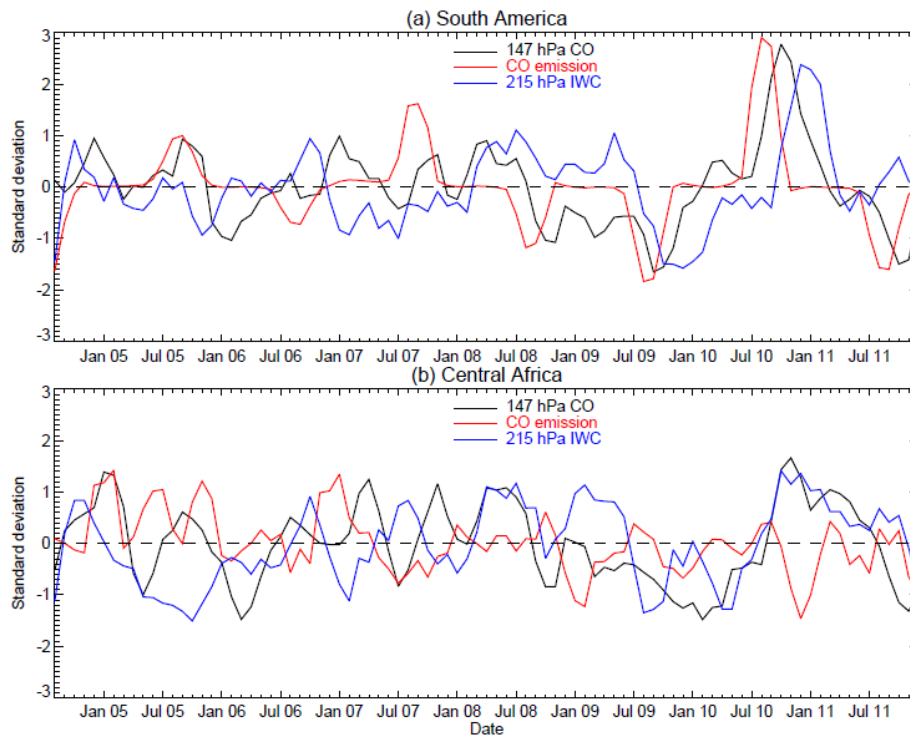


Fig. 4. Time series of monthly anomalies of MLS CO at 147 hPa (black), surface CO emission (red) and MLS ice water content (IWC) at 215 hPa over **(a)** South America (15°S – 12°N , 85°W – 32°W) and **(b)** Central Africa (15°S – 15°N , 20°W – 50°E) for the period of August 2004–December 2011.

Impacts of fire emissions and transport pathways

L. Huang et al.

Title Page

Abstract

Introduction

Conclusions

References

Tables

Figures

◀

▶

◀

▶

Back

Close

Full Screen / Esc

Printer-friendly Version

Interactive Discussion

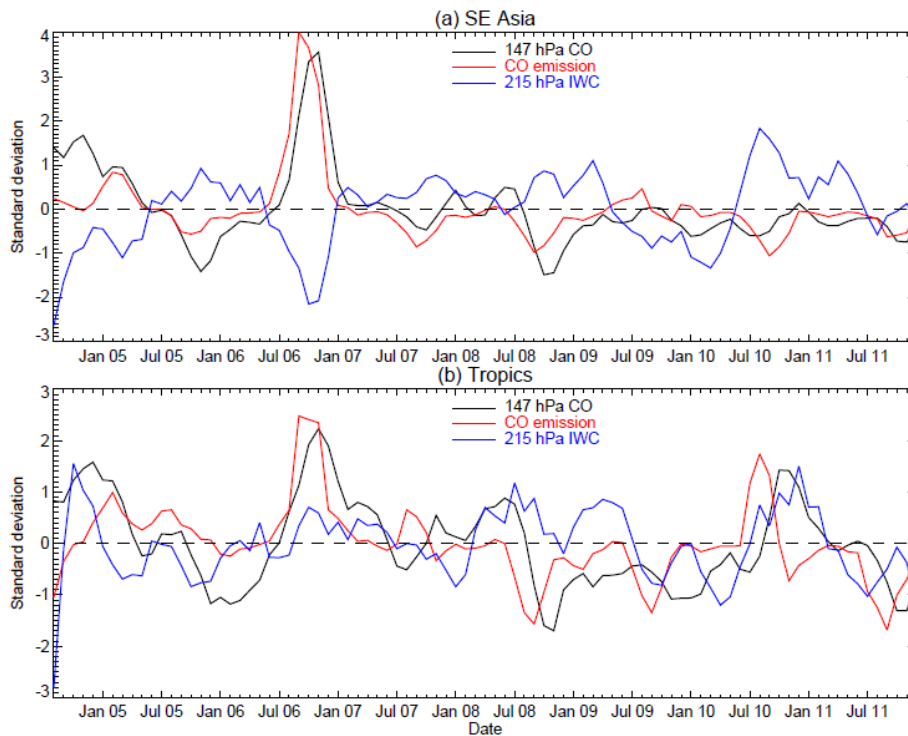


Fig. 5. As in Fig. 4, but for **(a)** SE Asia (10° S– 15° N, 90° E– 160° E); **(b)** Tropics (15° S– 15° N, 180° W– 180° E).

Impacts of fire emissions and transport pathways

L. Huang et al.

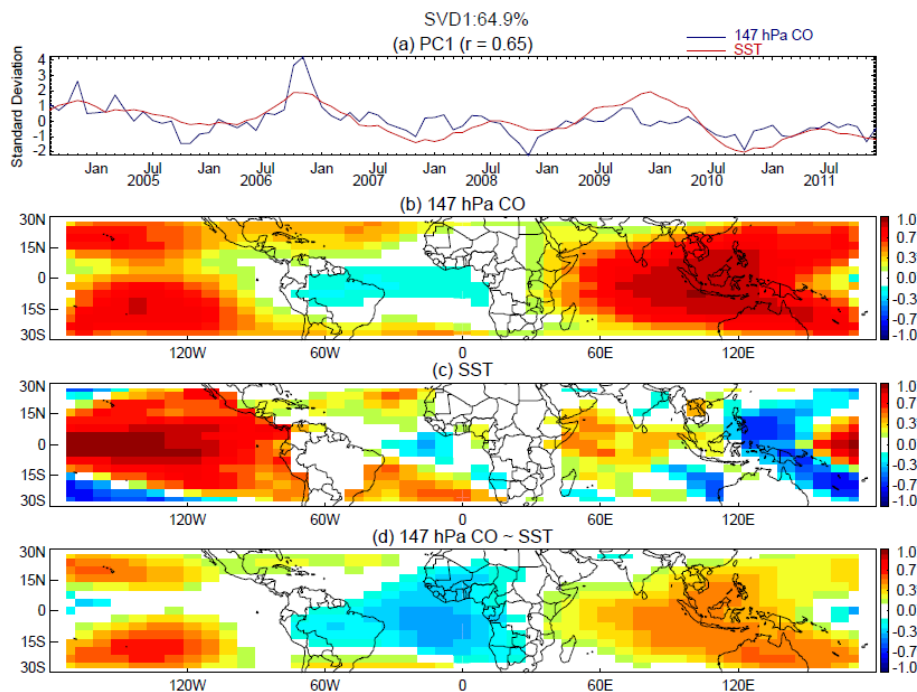


Fig. 6. (a) Principle components of 147 hPa CO (blue) and SST (red), (b) homogeneous correlation map for 147 hPa CO, (c) homogeneous correlation map for SST, (d) heterogeneous correlation map for 147 hPa CO, of the first SVD mode of 147 hPa CO and SST for the period of August 2004–December 2011.

[Title Page](#)[Abstract](#)[Introduction](#)[Conclusions](#)[References](#)[Tables](#)[Figures](#)[◀](#)[▶](#)[◀](#)[▶](#)[Back](#)[Close](#)[Full Screen / Esc](#)[Printer-friendly Version](#)[Interactive Discussion](#)

Impacts of fire emissions and transport pathways

L. Huang et al.

Title Page

Abstract

Introduction

Conclusions

References

Tables

Figures

◀

▶

◀

▶

Back

Close

Full Screen / Esc

Printer-friendly Version

Interactive Discussion

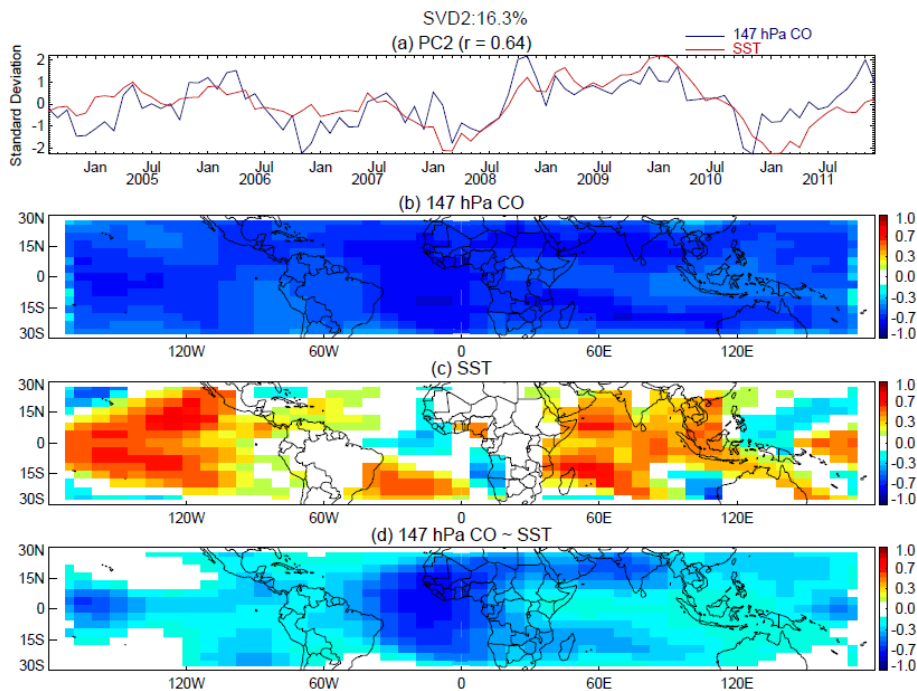


Fig. 7. As in Fig. 6, but for the second SVD mode of 147 hPa CO and SST.

Impacts of fire emissions and transport pathways

L. Huang et al.

Title Page

Abstract

Introduction

Conclusions

References

Tables

Figures

◀

▶

◀

▶

Back

Close

Full Screen / Esc

Printer-friendly Version

Interactive Discussion

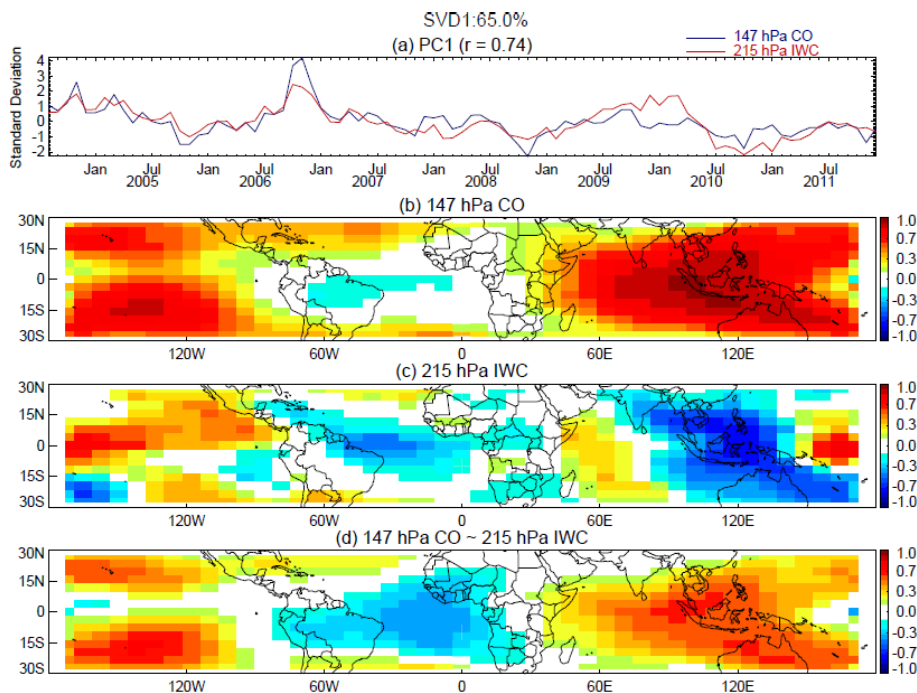


Fig. 8. (a) Principle components of 147 hPa CO (blue) and 215 hPa IWC (red), (b) homogeneous correlation map for 147 hPa CO, (c) homogeneous correlation map for 215 hPa IWC, (d) heterogeneous correlation map for 147 hPa CO, of the first SVD mode of 147 hPa CO and 215 hPa IWC for the period of August 2004–December 2011.

Impacts of fire emissions and transport pathways

L. Huang et al.

Title Page

Abstract

Introduction

Conclusions

References

Tables

Figures

◀

▶

◀

▶

Back

Close

Full Screen / Esc

Printer-friendly Version

Interactive Discussion

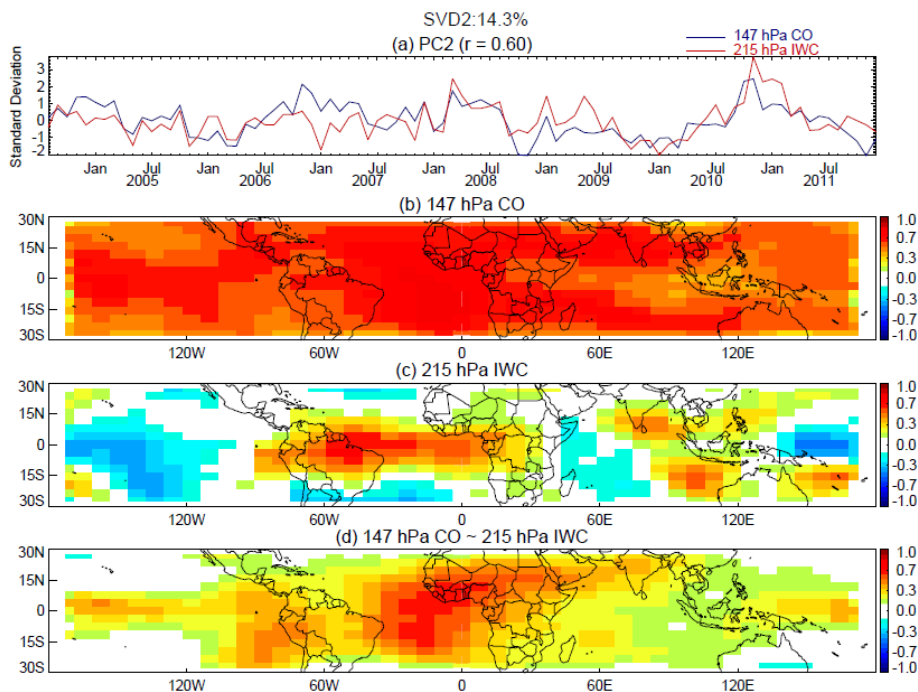


Fig. 9. As in Fig. 8, but for the second SVD mode of 147 hPa CO and 215 hPa IWC.

Impacts of fire emissions and transport pathways

L. Huang et al.

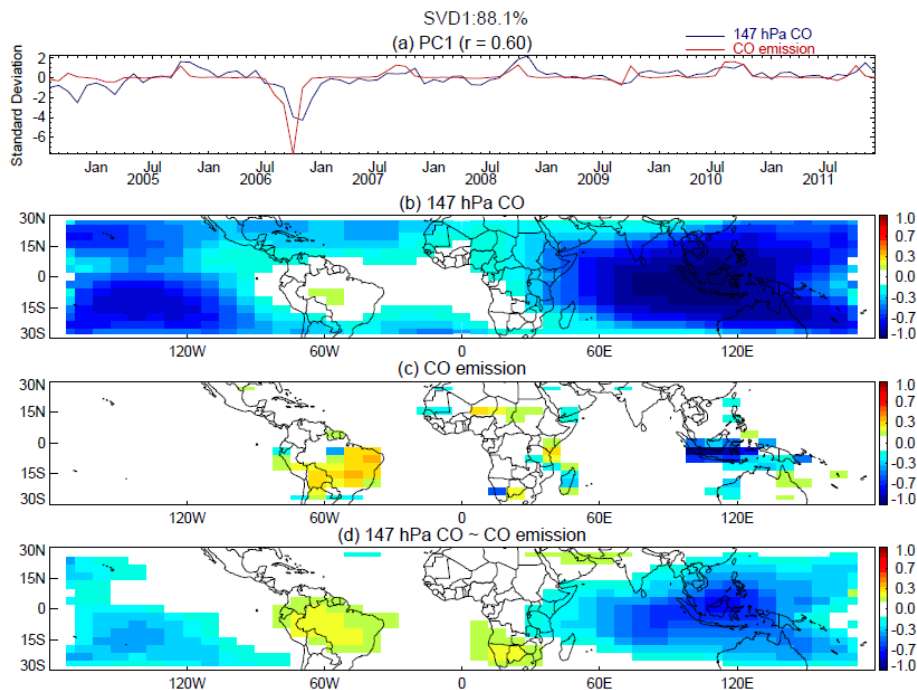


Fig. 10. (a) Principle components of 147 hPa CO (blue) and surface CO emission (red), (b) homogeneous correlation map for 147 hPa CO, (c) homogeneous correlation map for surface CO emission, (d) heterogeneous correlation map for 147 hPa CO, of the first SVD mode of 147 hPa CO and surface CO emission for the period of August 2004–December 2011.

Impacts of fire emissions and transport pathways

L. Huang et al.

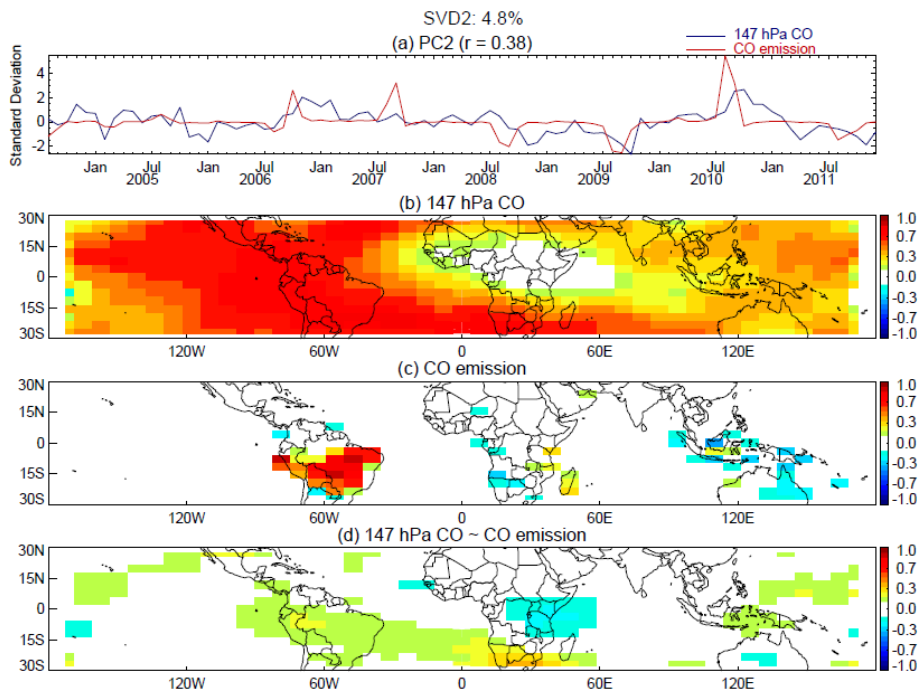


Fig. 11. As in Fig. 10, but for the second SVD mode of 147 hPa CO and surface CO emission.

[Title Page](#)[Abstract](#)[Introduction](#)[Conclusions](#)[References](#)[Tables](#)[Figures](#)[◀](#)[▶](#)[◀](#)[▶](#)[Back](#)[Close](#)[Full Screen / Esc](#)[Printer-friendly Version](#)[Interactive Discussion](#)

Impacts of fire emissions and transport pathways

L. Huang et al.

Title Page

Abstract

Introduction

Conclusions

References

Tables

Figures

◀

▶

◀

▶

Back

Close

Full Screen / Esc

Printer-friendly Version

Interactive Discussion

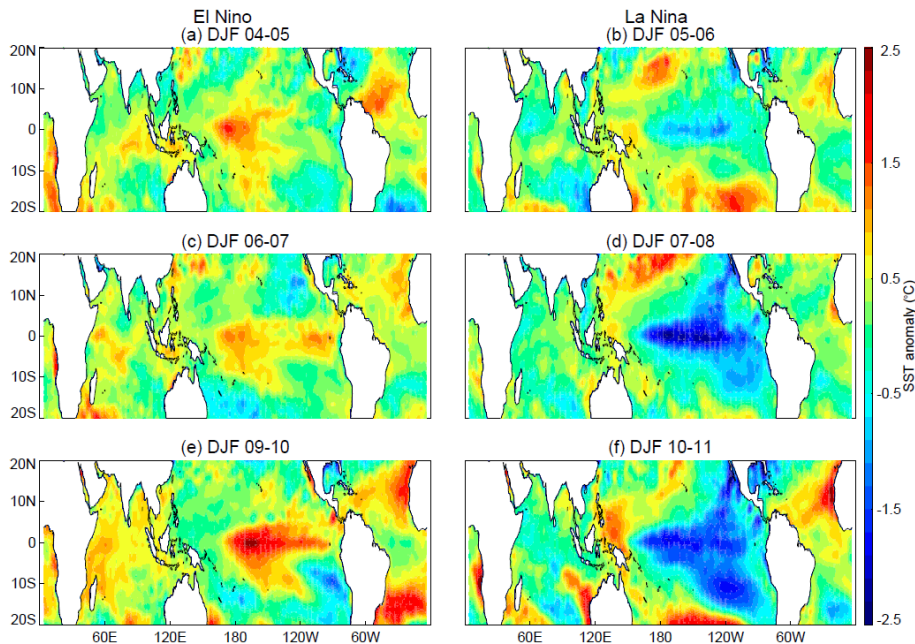


Fig. 12. Seasonal (DJF) mean distributions of SST anomaly during **(a)** 2004–2005, **(b)** 2005–2006, **(c)** 2006–2007, **(d)** 2007–2008, **(e)** 2009–2010 and **(f)** 2010–2011.

Impacts of fire emissions and transport pathways

L. Huang et al.

Title Page

Abstract

Introduction

Conclusions

References

Tables

Figures

◀

▶

◀

▶

Back

Close

Full Screen / Esc

Printer-friendly Version

Interactive Discussion

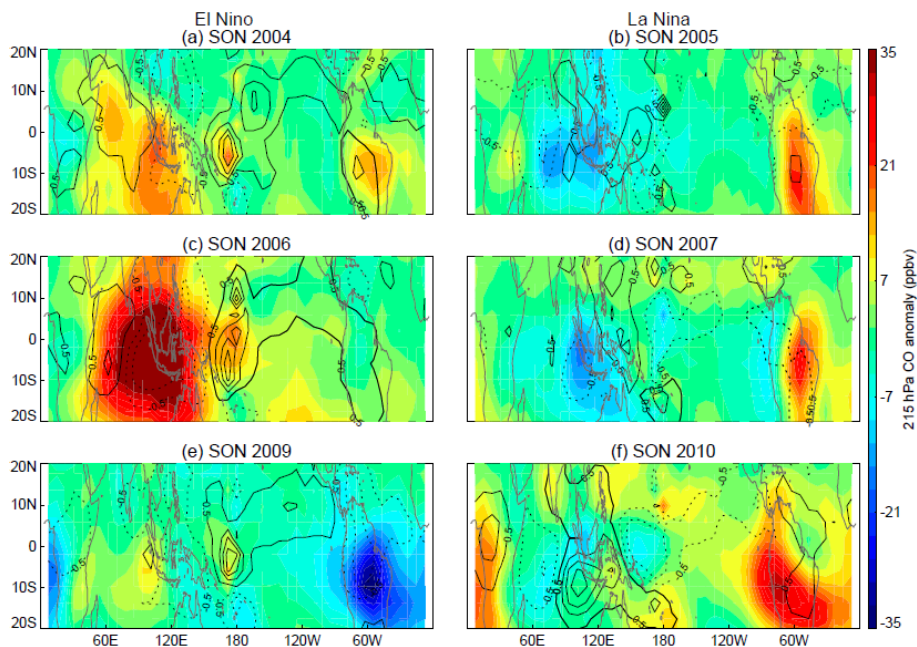


Fig. 13. Seasonal (SON) mean distributions of CO (shaded contour) and IWC (line contour) anomalies in the upper troposphere (215 hPa) during **(a)** 2004, **(b)** 2005, **(c)** 2006, **(d)** 2007, **(e)** 2009 and **(f)** 2010. The IWC contour interval is 1 mg m^{-3} . The solid line represents positive IWC anomaly, and the dotted line represents negative IWC anomaly.

Impacts of fire emissions and transport pathways

L. Huang et al.

Title Page

Abstract

Introduction

Conclusions

References

Tables

Figures

◀

▶

◀

▶

Back

Close

Full Screen / Esc

Printer-friendly Version

Interactive Discussion

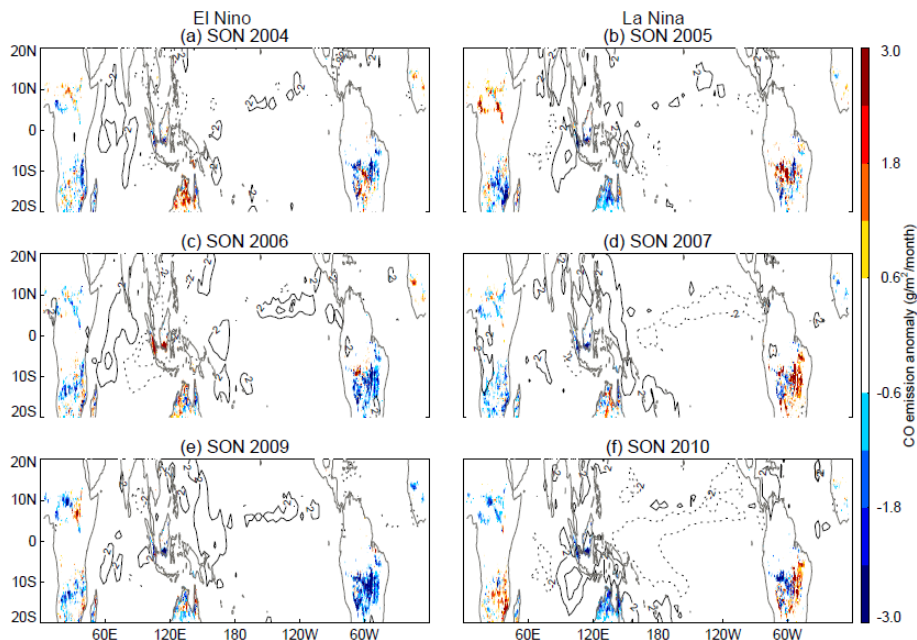


Fig. 14. As in Fig. 13, but for surface CO emission (shaded contour) and precipitation (line contour) anomalies. The precipitation contour interval is 4 mm d^{-1} . The solid line represents positive precipitation anomaly, and the dotted line represents negative precipitation anomaly.

Impacts of fire emissions and transport pathways

L. Huang et al.

Title Page

Abstract

Introduction

Conclusions

References

Tables

Figures

◀

▶

◀

▶

Back

Close

Full Screen / Esc

Printer-friendly Version

Interactive Discussion

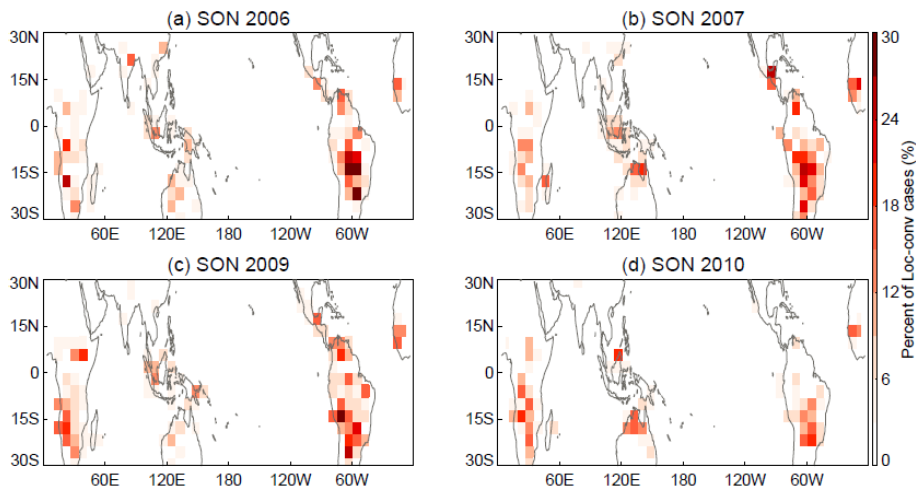


Fig. 15. Spatial distributions of the relative frequency (percentage) of the “local convection” transport pathway within each 4° latitude \times 8° longitude grid box during **(a)** SON 2006, **(b)** SON 2007, **(c)** SON 2009 and **(d)** SON 2010.

Impacts of fire emissions and transport pathways

L. Huang et al.

Title Page

Abstract

Introduction

Conclusions

References

Tables

Figures

◀

▶

◀

▶

Back

Close

Full Screen / Esc

Printer-friendly Version

Interactive Discussion

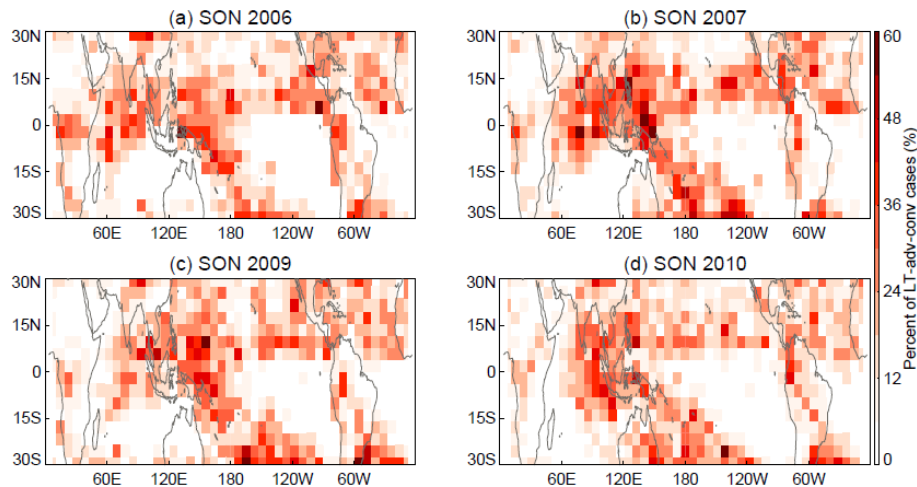


Fig. 16. As in Fig. 15, but for the “LT advection → convection” transport pathway.

Impacts of fire emissions and transport pathways

L. Huang et al.

Title Page

Abstract

Introduction

Conclusions

References

Tables

Figures

◀

▶

◀

▶

Back

Close

Full Screen / Esc

Printer-friendly Version

Interactive Discussion

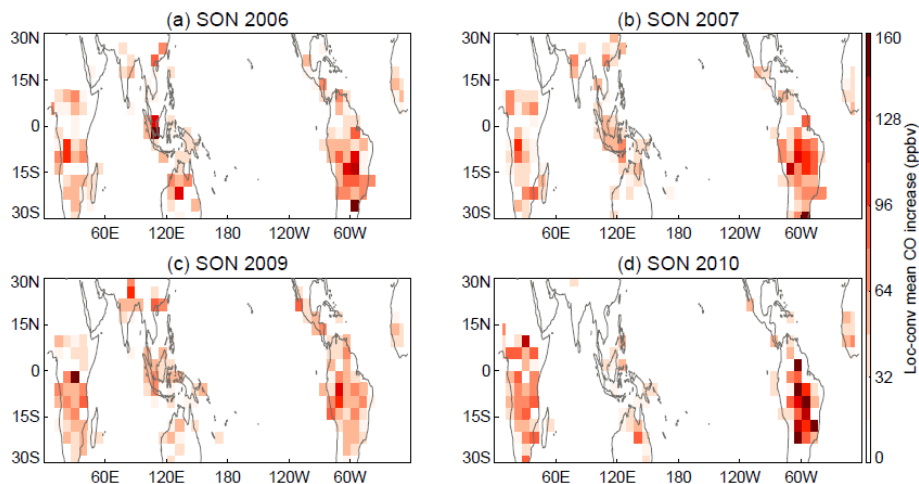


Fig. 17. Spatial distributions of the average increase of CO associated with the “local convection” transport pathway within each 4° latitude \times 8° longitude grid box during (a) SON 2006, (b) SON 2007, (c) SON 2009 and (d) SON 2010.

Impacts of fire emissions and transport pathways

L. Huang et al.

Title Page

Abstract

Introduction

Conclusions

References

Tables

Figures



Back

Close

Full Screen / Esc

Printer-friendly Version

Interactive Discussion

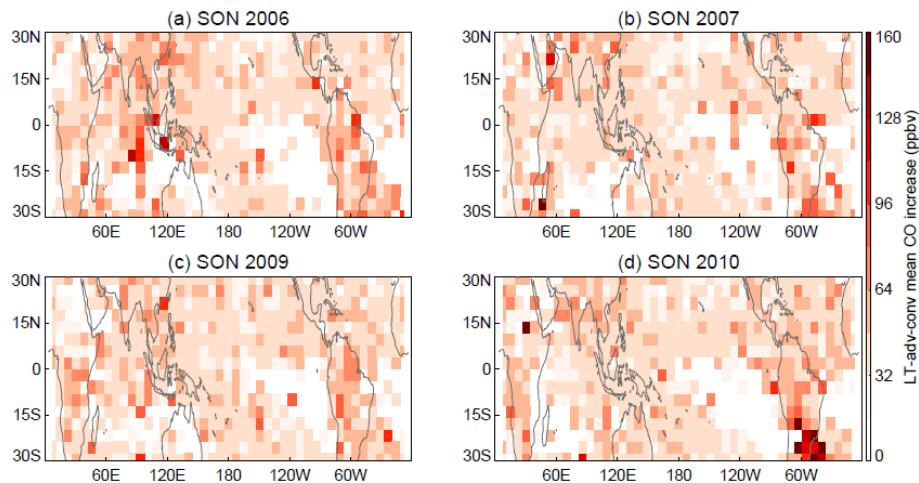


Fig. 18. As in Fig. 17, but for the “LT advection \rightarrow convection” transport pathway.